DEVELOPMENT OF A PORTABLE LOW-MOISTURE FOOD PASTEURIZATION DEVICE USING RF HEATING

A Thesis

presented to

the Faculty of California Polytechnic State University,

San Luis Obispo

In Partial Fulfillment

of the Requirements for the Degree

Master of Science in Electrical Engineering

by

Eric Ohata

June 2021

COMMITTEE MEMBERSHIP

TITLE: Development of a Portable Low-Moisture Food Pasteurization Device Using RF Heating

AUTHOR: Eric Ohata

DATE SUBMITTED: June 2021

COMMITTEE CHAIR: Dean Arakaki, Ph.D.
Associate Professor of Electrical Engineering

COMMITTEE MEMBER: Marie Yeung, Ph.D.
Professor of Biological Sciences

COMMITTEE MEMBER: Steve Dunton, M.S.
Lecturer, Electrical Engineering

ABSTRACT

Development of a Portable Low-Moisture Food Pasteurization Device Using RF Heating

Eric Ohata

Bacterial presence in low-moisture foods such as flour, cereals, baby formula, and spices, have become a concern due to sanitizing challenges. The food industry currently focuses on wet food sanitation as opposed to low-moisture foods because of bacteria's inability to reproduce in low water activity media. Traditionally, food processing RF heating pasteurizes in mass quantities while an equivalent consumer device does not exist the market today. A consumer product would help eliminate food waste by providing an easy way to sanitize food and extend shelf life. The Portable Food Pasteurization (PFP) project is an interdisciplinary project involving the Electrical Engineering, Biology, and Food Science departments to develop an RF heating consumer device to pasteurize low-moisture foods. A prototype device was designed but construction was delayed because of the COVID-19 pandemic. We are continuing this project by replacing the previously designed MOSFET inverter with a class C amplifier due to parts availability and performance. The food chamber is redesigned by Jonathan Souza to incorporate parallel plate electrodes for more uniform heating without risk of burning. Tim Erwin improved the flyback converter with a snubber and discharge circuit. Tradeoff analysis is performed on various system components to define a configuration for future development.

ACKNOWLEDGMENTS

I want to thank Jonathan Souza and Tim Erwin for their help with this project as well as Dr. Arakaki for his guidance and encouragement. I would like to thank Cal Poly's College of Engineering for sponsoring the project with the CP-Connect grant. This project would not be possible without their help.

Finally, I want to thank my family for their love and support throughout my time in this program. I could not have gotten through this without them.

TABLE OF CONTENTS

Page

LIST OF TABLES viii
LIST OF FIGURES ix
CHAPTER
1. Background 1
1.1. Bacteria Growth in Low-Moisture Foods 1
2. System Overview 4
3. Flyback Converter 6
3.1. Flyback Converter vs. Boost Converter 6
3.2. Flyback Converter Operating Principles 7
3.3. Snubber Circuit 8
3.4. Discharge Circuit 11
3.5. Flyback Design 12
3.6. Flyback Converter LTSPICE Simulation 14
4. Class C Amplifier 16
4.1. Self-Excited vs. External Frequency Reference Configurations 16
4.1.1. External Frequency Reference Circuit 16
4.1.2. Self-Excited Circuit 18
4.2. Amplifier Design 20
5. Food Chamber 24
5.1. Parallel Plate vs. Cylindrical Container 24
5.1.1. Food Position Within the Chamber 26
5.2. Equivalent Circuit Model 28
5.3. Food Chamber 30
5.4. Parallel Plate Breakdown Voltage 31
6. Experimental Results 34
6.1. Flyback Converter 34
6.2. Class C Amplifier 35
6.3. Food Chamber 37
7. Conclusions And Future Work 40

7.1. Tradeoff Analysis Summary 40
7.2. Future Work 41
REFERENCES 43
APPENDICES
A. LT3751 Datasheet Schematic 45
B. Flyback Converter Schematics and PCB 46
C. Class C Amplifier Schematic and PCB 50
D. Flyback Converter BOM 53
E. Class C Amplifier BOM 54
F. Food Chamber BOM 55

LIST OF TABLES

Table Page

1. Component Values for Flyback Converter 14

2. Final Design Values for Class C Amplifier 21

3. Food Chamber Parameters 29

4. Computed k as a Function of pd [18] 32

5. System Tradeoffs 41

LIST OF FIGURES

Figure Page

1. PSC 200kW RF/Convection Dryer (Source: [6]) 3

2. Food Pasteurization System 4

3. Flyback Converter, "On" State 7

4. Flyback Converter, "Off" State 7

5. Flyback Converter With Snubber (R1, C1, D2) 9

6.Snubber Circuit, C_1 Voltage Waveform, One Cycle 9

7. Flyback Discharge Circuit 11

8.Flyback Converter Schematic [10] 12

9.Flyback Converter Output Voltage Start-Up Characteristic 14

10. Flyback Converter Input Current 15

11. External Reference Class C Amplifier 17

12. External Reference Circuit Total Current Draw 18

13. Self-Exciting Class C Amplifier 19

14. Class C Amplifier Schematic 21

15. Class C Amplifier Output With Adjusted Component Values (Output 22

16. Input Current to Self-Excited Class C Amplifier 22

17. Cylindrical Chamber Design [2] 24

18. Cylindrical Container Top-Down View 25

19. Electric Field Strength Between Parallel Plates (a) no dielectric sample, (b) dielectric sample centered on bottom electrode, (c) dielectric sample placed in center between electrodes [12] 27

20. Parallel Plate Design Dimensions 30

21. Side View of Food Chamber and Aluminum Shielding 31

22. Constructed Flyback Converter 34

23. Flyback Converter Output Voltage 35

24. Modified Class C Amplifier 36

25. Modified Class C Amplifier Simulated Output Voltage 36

26. Class C Amplifier PCB 37

27. Food Chamber (Internal View) 38

28. Food Chamber (Side View) 38

29. LT3751 Block Diagram 45

30. Flyback Converter PCB Schematic 46

31. Flyback Converter PCB Layout (Top) 47

32. Flyback Converter PCB (Bottom) 48

33. Flyback Converter PCB Layout 49

34. Class C Amplifier PCB Schematic 50

35. Class C Amplifier PCB Layout (Top) 51

36. Class C Amplifier PCB Layout (Bottom) 52

Chapter 1: Background

Radio Frequency (RF) heating provides many advantages over other methods of reducing food borne pathogens. For example, thermal processing through heating coils increases food temperature to destroy bacteria. Although easy to implement, heat does not penetrate food effectively. Uneven distribution throughout the food leads to surface burning before the interior warms. Microwave heating has a similar problem; the short wavelength does not effectively penetrate large volumes of food [1]. RF heating is better suited for thermal pasteurization because its longer wavelength allows for deeper penetration and even temperature distribution without risk of burning.

In 2019, Joe Sandoval developed a system to pasteurize low-moisture foods using RF heating [2]. Due to the Covid-19 pandemic a prototype was never fully built. This year, a team led by myself aimed to expand and improve his design. The MOSFET inverter was replaced with a class C amplifier due to parts availability and performance. The flyback converter was improved by Tim Erwin with the addition of snubber and discharge circuits. Food chamber redesigns by Johnathan Souza include parallel plate electrodes for more uniform heating.

1.1 Bacteria Growth in Low-Moisture Foods

Water activity in food is defined by the ratio of water vapor pressure in food to the vapor pressure of pure water.

$$a_w = \frac{P}{P_0} \quad (1)$$

where P and P_0 are the vapor pressure of the food and pure water, respectively.

Low-moisture foods are defined by their low water activity ($a_w < 0.85$) [3]. Between low and high water activity foods, there is a higher risk for consumers to contract food borne diseases if they consume higher water activity food because it can support the growth foodborne pathogens. According to the United States Department of Agriculture (USDA), it is difficult for certain bacteria reproduce at temperatures below 40°F or above 140°F and the water activity is below 0.85 [4]. Although bacteria cannot reproduce, they can still be present and present a risk if consumed. To guarantee low-moisture foods are safe for consumption, they must be heated until there is at least a 5-log reduction in microbial load. A 5-log reduction is a benchmark for the Food and Drug Administration (FDA) to evaluate if a method can be considered an effective "kill" step [5]. Kill step is a term used to describe the moment where potentially harmful pathogens are eradicated from food. Treated food is safe for consumption when it can achieve a 5-log reduction in pathogens. Log reduction is defined by:

$$L = log_{10}\left(\frac{A}{B}\right) \quad (2)$$

where A and B are the number of bacteria before and after treatment, respectively.

In the food industry, RF heating techniques are used to pasteurize low-moisture products. RF heating (13.56MHz-40.68MHz) is preferred over traditional methods such as thermal processing and microwaves (2.45GHz)

because it preserves food quality more effectively [1]. Typically, devices used for RF heating are large and require hundreds of kW to operate (Fig. *1*).

Fig. 1: PSC 200kW RF/Convection Dryer (Source: [6])

These devices utilize frequencies within the industrial, scientific, and medical (ISM) band. The FCC allows 13.56MHz, 27.12MHz, and 40.68MHz for commercial purposes. For this project 13.56MHz was chosen because it has the longest wavelength at 22.1m. Previous efforts presumed longer wavelengths provide a greater depth of penetration which heats food more evenly [7].

Chapter 2: System Overview

The RF pasteurization device outlined in this paper includes 4 major components: an off-the-shelf 24V power supply, a flyback DC-DC converter, a class C amplifier, and the food sample chamber.

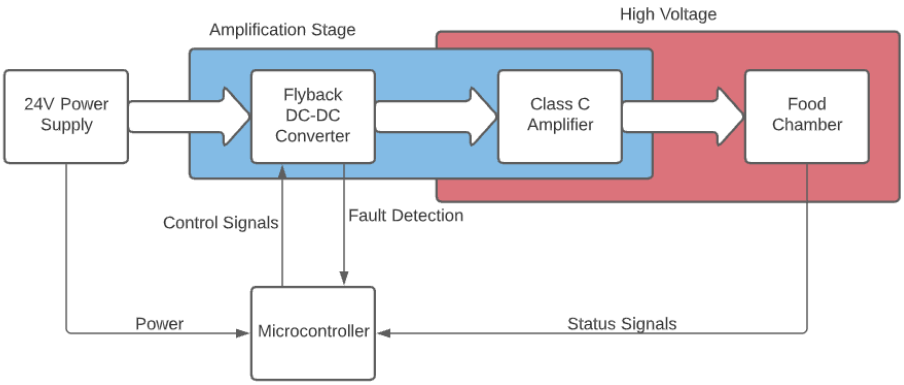

Fig. 2: Food Pasteurization System

The 24V power supply biases both the flyback DC-DC converter and the microcontroller with a maximum current output of 20A.

The amplification stage includes the flyback DC-DC converter and the class C amplifier. The DC-DC unit converts a 24V input to a 200V DC output. Control signals from the LT3751 flyback controller's charge and fault pins will be monitored by an external microcontroller to disable the circuit when not in use. Due to the high voltage flyback converter output, fault detection is necessary to ensure safe operation. If overcurrent or overloading of the circuit is detected, the microcontroller will disable the circuit to prevent system damage.

The 200VDC flyback converter output is applied to a class C amplifier to modulate the DC voltage into a 13.56MHz half-rectified sine wave suitable for

RF heating. An LC tank circuit is used to tune the amplifier's output frequency and the resulting waveform is applied to the food chamber.

The food chamber consists of a parallel plate capacitor and metal shielding to protect against unwanted RF radiation (Fig. *21*). Food is placed between the two plates for pasteurization.

Chapter 3: Flyback Converter

To generate a high voltage DC source, a boost converter is used to increase the 24V DC supply to 200V DC. A flyback converter was chosen for its ability to output a large DC voltage without the need for a large power supply.

3.1 Flyback Converter vs. Boost Converter

Two popular options are available for increasing a DC voltage: flyback and boost converters. Both circuits operate similarly with one difference: the boost and flyback converters utilize an inductor and flyback transformer, respectively. Given the same input voltage, the transformer allows the flyback circuit to generate a larger output by utilizing the turns ratio. The flyback transformer also isolates the low from the high voltage sections. If either side fails, the other half is protected from damage.

3.2: Flyback Converter Operating Principles

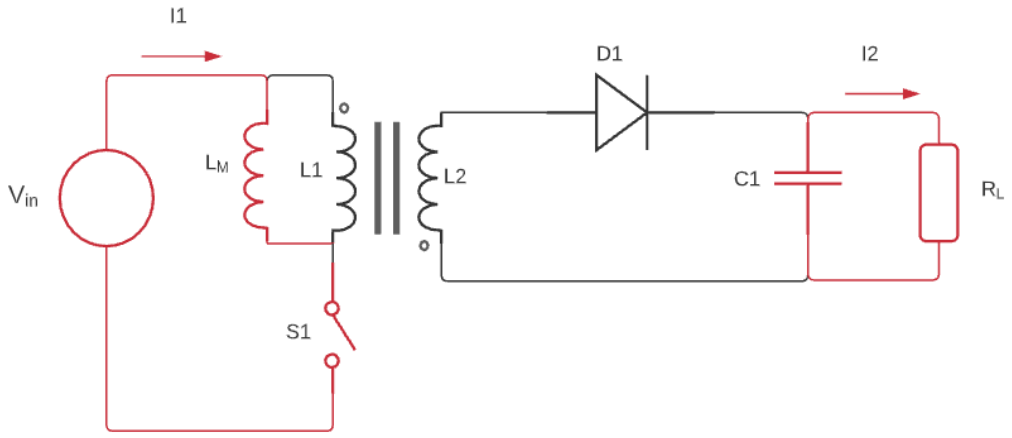

Fig. 3: Flyback Converter, "On" State

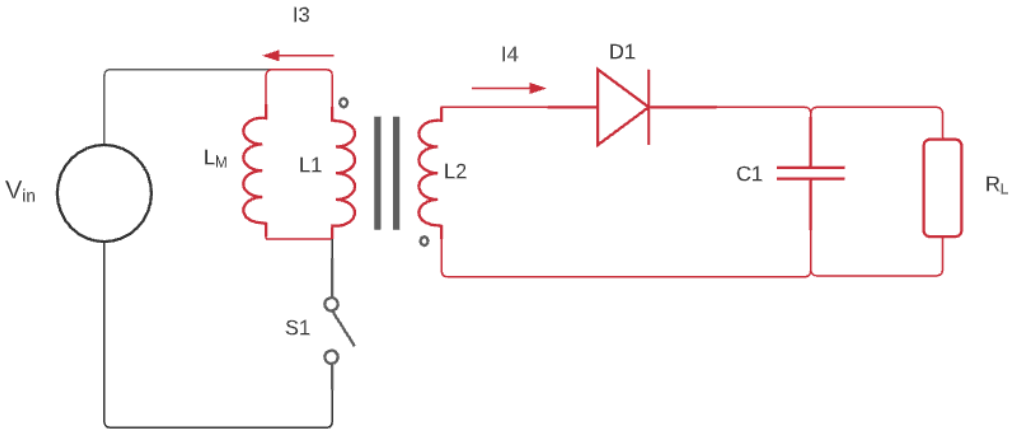

Fig. 4: Flyback Converter, "Off" State

The flyback converter switches between two states. The “on” state (Fig. *3*) when switch S1 is closed current, I_1 flows from V_{in} into the magnetizing inductor L_M which couples L1 to L2. Magnetic field energy is stored in L_M until the circuit switches to the “off” state. No current flows into inductor L_1 due to reverse-biased diode D1 on the secondary side. Any charge stored in C_1 is dissipated through the load during the “on” state.

The flyback converter changes into the "off" state when the switch S1 opens, and current flows from L_M into L_1. Current flows out of L_1 dot terminal, into L_2 dot. Diode D_1 allows current flow into both capacitor C_1 and the load. C_1 stores energy that is transferred to the load when the circuit returns to the "on" state.

Inductors L1 and L2 form a flyback transformer to increase voltage though mutual induction. The voltage increase is:

$$V_s = V_p \left(\frac{N_s}{N_p} \right) \tag{3}$$

where N_p and N_s are the primary and secondary coil turns, and V_p and V_s are the primary and secondary voltages. The Fig. *3* shows L1 and L2 are the primary and secondary, respectively. The turns ratio can be adjusted to increase the voltage to any desired value.

3.3 Snubber Circuit

During operation, the flyback converter can experience greater than the 20V maximum V_{gs} on the switching transistor (IPA95R450P7) during the "off" state [8] caused by residual energy stored in the transformer's leakage inductance L_M. One solution is to minimize transformer leakage inductance, but this requires a higher cost transformer. A more practical solution is to use a snubber circuit (Fig. 5) to limit transient voltage spikes by dissipating excess energy through a resistor.

The snubber circuit (resistor-capacitor-diode configuration) includes a Zener diode D1 and RC circuit. Zener diodes limit large voltage transients, and the RC circuit dissipates excess energy through R_1.

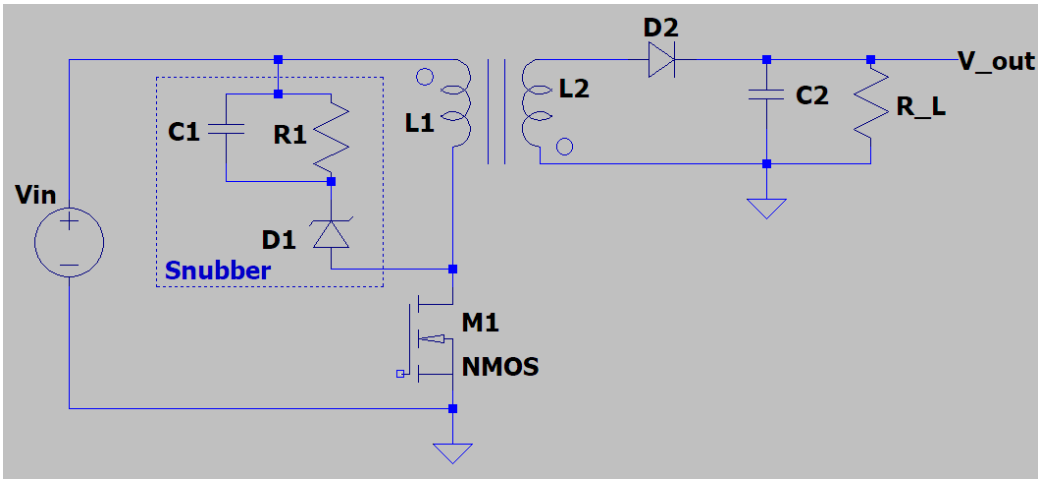

Fig. 5: Flyback Converter With Snubber (R1, C1, D2)

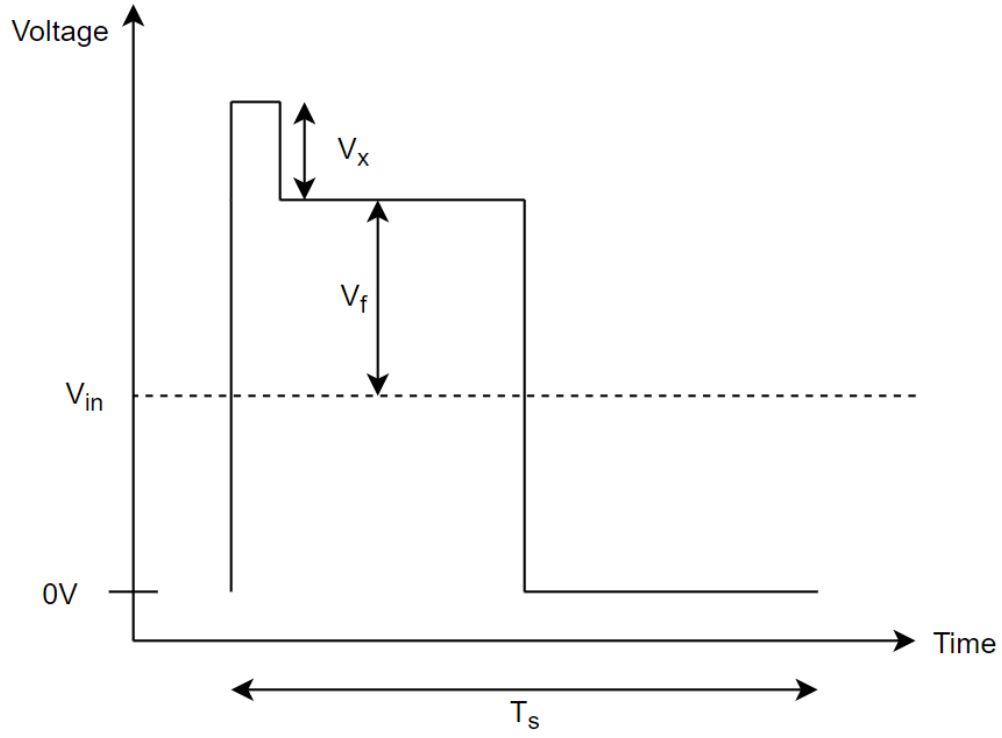

Fig. 6: Snubber Circuit, C_1 Voltage Waveform, One Cycle

The RCD snubber (Fig. *5*) includes a resistor, capacitor, and Zener diode (R_1, C_1, D_1). When MOSFET M1 is switched off, snubber circuit capacitor C_1 is charged to voltage V_f (Fig. *6*) defined by:

$$V_f = \frac{V_{out}}{N} + V_{in} \tag{4}$$

where N is the turns ratio (N_s/N_p).

Transformer leakage inductor stored power is [9]:

$$P_l = \frac{1}{2} L I_p^2 f_s \tag{5}$$

where L is leakage inductance, I_p is flyback inductor current, and f_s is the switching frequency. From (5), the maximum snubber dissipated power is [9]:

$$P_{sn}^{max} = P_l(1 + \frac{v_f}{v_x^{max}}) \tag{6}$$

P_{sn}^{max} is used to determine the maximum power rating for resistor R1. Typical designs set v_x to ½ V_f resulting in maximum dissipated power $3P_t$.

During switching, the voltage across C_1 also increases by an additional amount v_x (Fig. *6*). Voltage v_x is [9]:

$$v_x = \frac{1}{2}\left(\sqrt{v_f^2 + 2\frac{LI_p^2 R_1}{T_s}} - v_f\right) \tag{7}$$

where T_s is the switching period (Fig. *6*). Snubber circuit power dissipation is [9]:

$$P_{sn} = \frac{\left(v_x + v_f\right)^2}{R_1} \tag{8}$$

Capacitor C_1 maintains a constant voltage V_{in} while containing the leakage energy over each switching cycle.

3.4 Discharge Circuit

A discharge circuit is added at the flyback output to remove any remaining charge on the output capacitors after the converter is turned off.

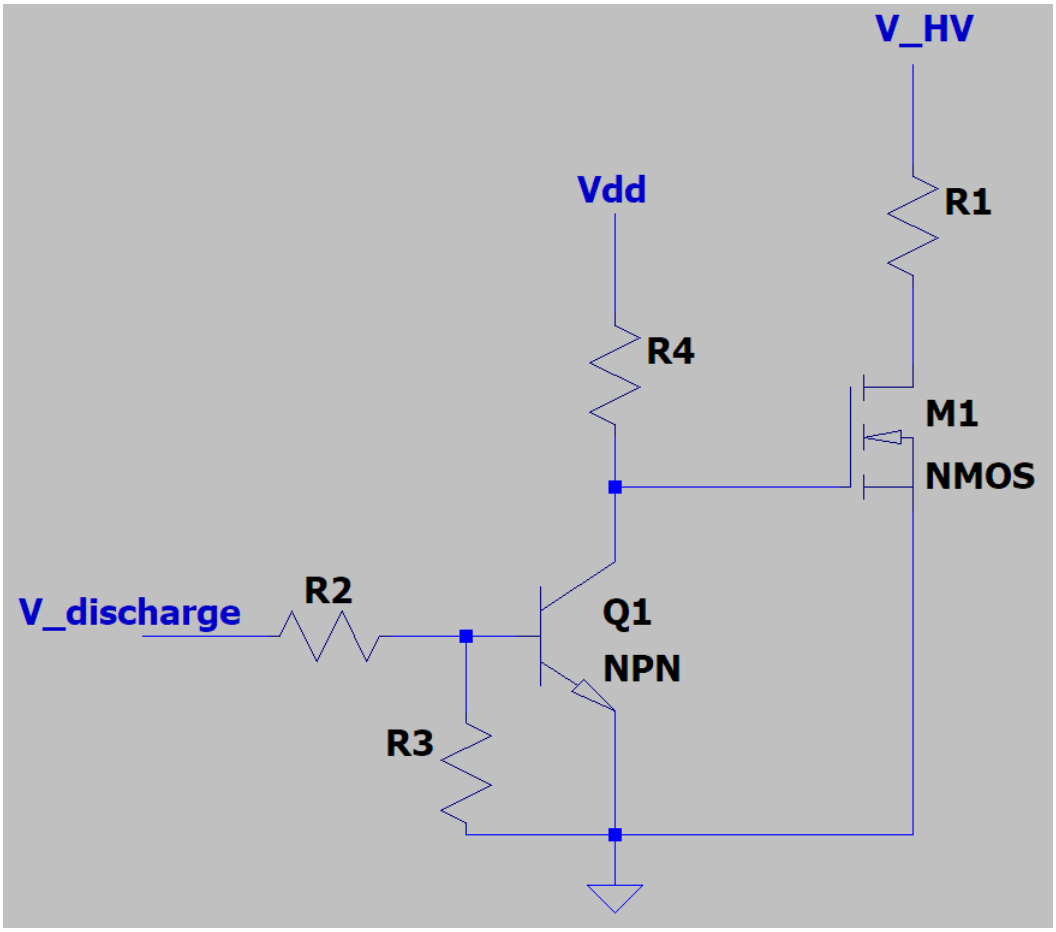

Fig. 7: Flyback Discharge Circuit

The high voltage flyback converter output is connected at V_{HV}. $V_{discharge}$ is controlled by an external microcontroller and remains at 0V when the flyback converter is operating. When $V_{discharge}$ is 0V, Q1 and M1 are both off and do not conduct current; the discharge circuit is inactive, and the flyback converter functions normally.

When $V_{discharge}$ is set high (3.3V), Q1 turns on and applies V_{dd} to M1 gate. M1 shorts R1 to ground and discharges the flyback output capacitors (see Fig. *5*).

3.5 Flyback Design

To implement the flyback converter, the LT3751 flyback controller is used regulate the circuit. This project utilizes the LT3751 low noise regulator configuration (Fig. *8*). The flyback transformer uses a 1:10 turns ratio.

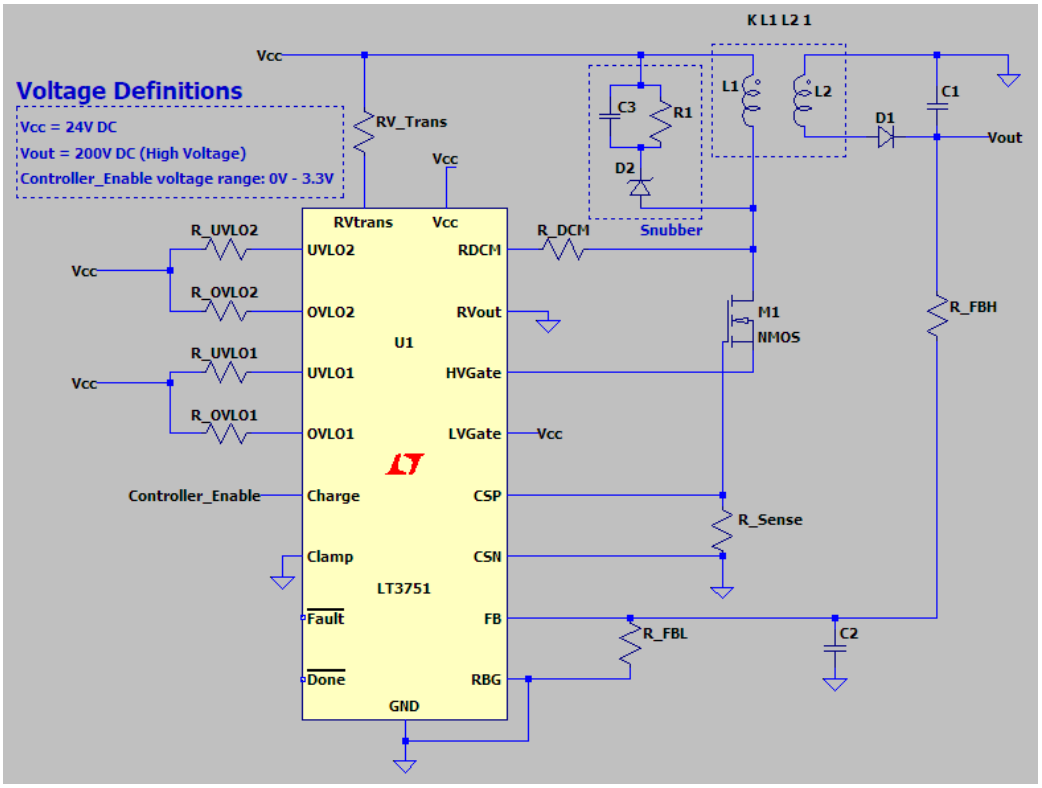

Fig. 8: Flyback Converter Schematic [10]

The LT3751 maximum output current is 270mA [10]. The resistor and capacitor values for the flyback converter are determined using equations and recommendations in the LT3751 datasheet [10]. Capacitances on resistors are minimized to V_{out} and R_{DCM} comparator response times. Ground pads and power

planes on the bottom of the PCB are removed from under RV_{trans} and R_{DMC} to minimize capacitance further.

The LT3751's low noise regulation mode requires the use of feedback resistors. High and low feedback resistors R_{FBH} and R_{FBL} are chosen based on the power dissipation and desired output voltage [10]:

$$R_{FBH} = \frac{(V_{Out} - 1.22)^2}{P_D} \tag{9}$$

$$R_{FBL} = \left(\frac{1.22}{V_{Out} - 1.22}\right) \cdot R_{FBH} \tag{10}$$

where V_{out} is the output voltage and P_D is the power rating of R_{FBH}.

A minimum load current is required to prevent the LT3751 from entering no-load operation [10]:

$$I_{Load(Min)} \geq \frac{L_{PRI} \cdot I_{PK}^2 \cdot 23kHz}{100 \cdot V_{Out}} \tag{11}$$

where L_{PRI} is the transformer primary inductance and I_{pk} is the peak primary current at maximum power delivery.

All component values were chosen using equations and tables from [10].

Table 1: Component Values for Flyback Converter

Component	Value
RV_{Trans}	40.2kΩ
R_{UVLO1}	432kΩ
R_{UVLO2}	475kΩ
Ro_{VLO1}	432kΩ
Ro_{VLO2}	475kΩ
R_{DCM}	18.2kΩ
R_{Sense}	6mΩ
R_{FBH}	124kΩ
R_{FBL}	768Ω
L1	2.5µH
L2	0.25µH
C2	10nF

3.6 Flyback Converter LTSPICE Simulation

The circuit defined in Fig. *8* was simulated in LTSPICE with the values from Table *1* to verify operation.

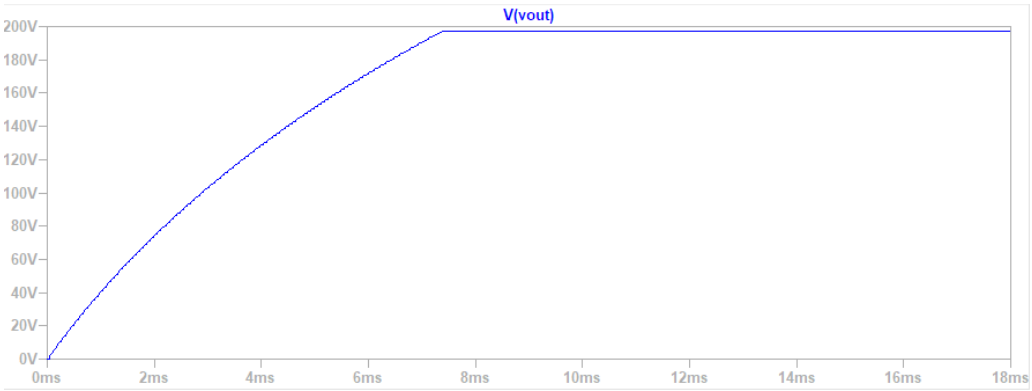

Fig. 9: Flyback Converter Output Voltage Start-Up Characteristic

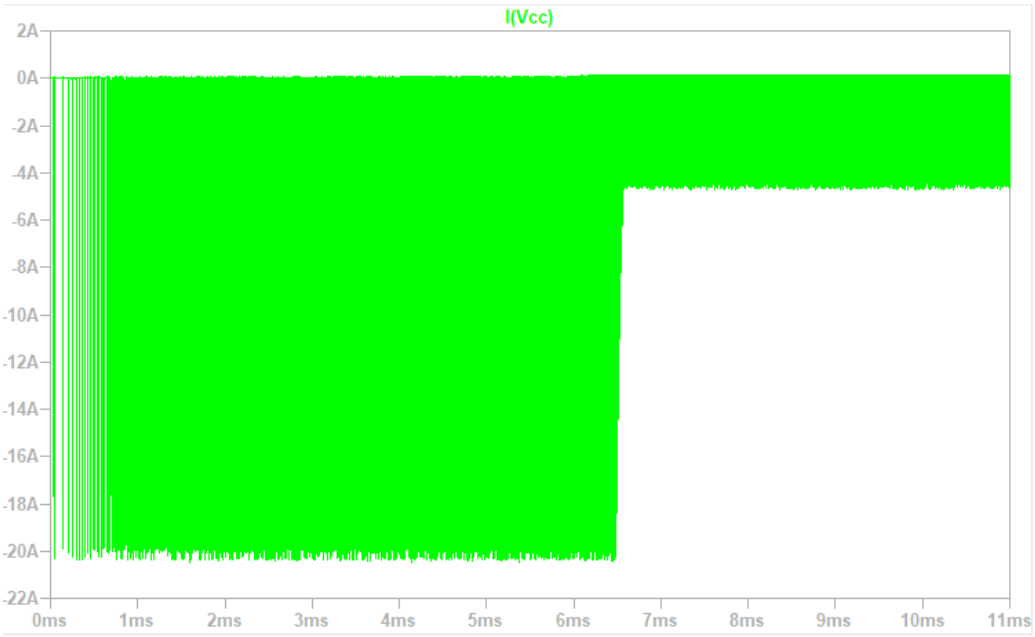

Fig. 10: Flyback Converter Input Current

The flyback converter output voltage reaches a steady state of 197.45V DC at 7.4ms after startup (Fig. *9*). Initially, the flyback converter draws 20A peak from the 24V power source (Fig. *10*). This is the natural response of the circuit and independent of the 20A limited power supply. After entering steady state, the current reduces to 4A peak.

Chapter 4: Class C Amplifier

To modulate the 200V DC output of the flyback converter, a class C amplifier was chosen for its tunable frequency and high efficiency [11].

Class C amplifiers are denoted by their parallel resonance circuits and small conduction angle ($\theta < 180°$). The parallel resonant circuit allows the amplifier to operate at a specific frequency, making it suitable for RF applications.

4.1 Self-Excited vs. External Frequency Reference Configurations

Class C amplifiers are self-excited or require an external frequency reference. The external frequency reference is an AC control voltage tuned exactly to the resonant frequency of the tank circuit. On the other hand, the self-excited circuit can operate with only a single DC voltage source and no control signal.

4.1.1 External Frequency Reference Circuit

The external frequency reference configuration requires an AC input voltage with a DC bias, as well as a resonant circuit (Fig. *11*).

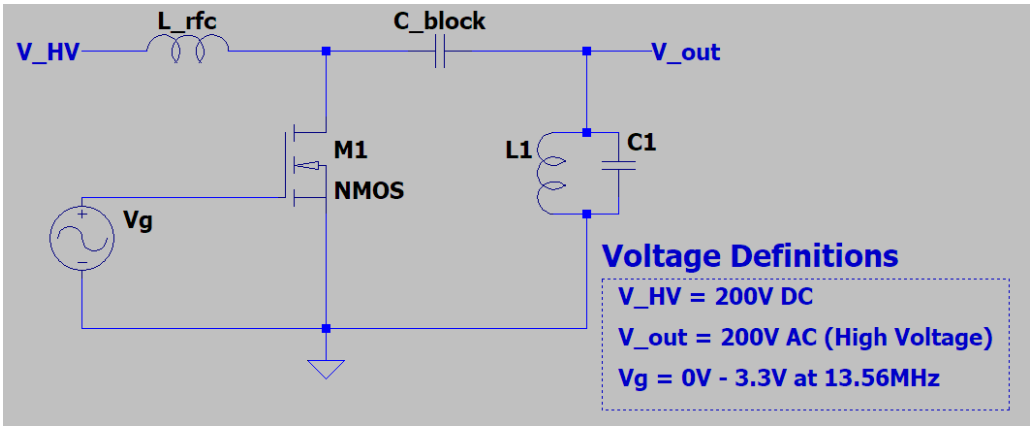

Fig. 11: External Reference Class C Amplifier

V_{dd} is the circuit's high voltage source while Vg is the control voltage that determines the operating frequency. L1 and C1 form the tank circuit and its resonant frequency is:

$$f = \frac{1}{2\pi\sqrt{L_1 C_1}} \tag{12}$$

The tank circuit's resonant frequency and the frequency of V_g must match as closely as possible to avoid unwanted modulation. If either components' frequencies differ, it could cause destructive interference and result in a decreased output voltage amplitude.

C_{block} is used to eliminate any DC bias from V_{out}. The value of C_{block} is selected to avoid a high impedance at the operating frequency. From [11], C_{block} is:

$$\frac{1}{2\pi f \cdot C_{block}} < 50\Omega \tag{13}$$

L_{rfc} is an RF choke used to prevent the high frequency output signal from shorting through the high voltage DC source.

Although this design is simple, it would not work at the high voltages that are required for this project. The large voltage across the M1 causes a large current through the MOSFET's drain.

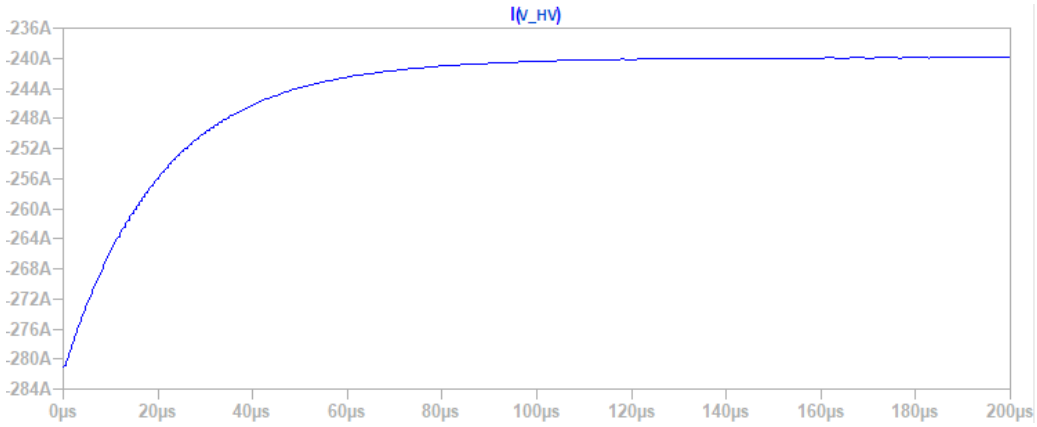

Fig. 12: External Reference Circuit Total Current Draw

With V_{dd} at 200V, an operating frequency of 13.56MHz, and no load, the non-self-exciting circuit draws a constant 240A from the voltage source. With no load, all the current is wasted as heat though the MOSFET. The circuit's large current draw is impractical to implement into a real product. Therefore, a different design must be considered for practical use.

4.1.2 Self-Excited Circuit

The other type of class C amplifier is the self-excited type. This circuit can operate with only one voltage source as opposed to two used by the non-self-excited type.

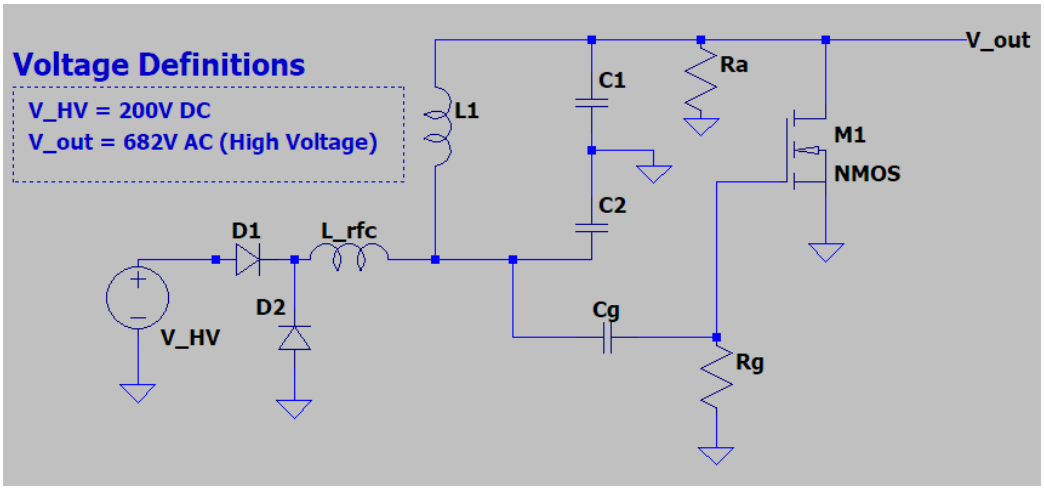

Fig. 13: Self-Exciting Class C Amplifier

Rather than a tank circuit consisting of one inductor and one capacitor, the self-excited type utilizes a Colpitts oscillator. The oscillator's operating frequency is:

$$f = \frac{1}{2\pi\sqrt{L_1 C_{eq}}} \tag{14}$$

where C_{eq} is the series combination of C_1 and C_2:

$$C_{eq} = \frac{C_1 * C_2}{C_1 + C_2} \tag{15}$$

Compared to the non-self-excited type, no external control signal is required to switch the MOSFET. The switching signal comes from there Colpitts oscillator itself and is connected to the MOSFET's gate through capacitor Cg. As the tank circuit oscillates, the MOSFET switches on and off creating a modulating output voltage.

MOSFET gates are sensitive to large voltage spikes and must be kept below the maximum rated voltage to avoid damage. Capacitor C_g protects the MOSFET's gate from the tank circuit's high voltage. Resistor R_g is used remove

any buildup of charge over C_g. If R_g was not present, the capacitor would build up charge over time and the voltage across C_g would cease to oscillate.

RFC is a choke that protects the Colpitts oscillator AC voltage from shorting to the DC supply. Diodes D1 and D2 are used for reverse current protection to avoid damage to the flyback converter.

The resistor R_a is used to discharge the capacitor C_1. If R_a were not present in the circuit, charge would build up over C_1 and the tank circuit would stop oscillating. In the final design, R_a is lumped into the equivalent load circuit (Fig. *14*).

Originally, the class C amplifier was meant to operate with an input voltage of 300V. This caused the output voltage to reach a peak of more than 1kV. The current draw form the flyback converter was around 800mA, much greater than what the flyback could deliver. To combat this problem, the input voltage was reduced to 200V, causing the output voltage to decrease to 670V and the input current to decrease to 130mA. The lower voltage is easier for PCB design and the lower current grants a larger margin if extra current is required from the flyback converter.

4.2 Amplifier Design

Amplifier component values from [11] and the Fig. *13* circuit. The circuit operates at 8.7MHz, lower than the 13.56MHz required. Improper values for

Colpitts oscillator components cause the decay in voltage. Values for C_1, C_2, and L_1 were tuned until the desired frequency was achieved.

Table 2: Final Design Values for Class C Amplifier

Component	Value
C_1	5pF
C_2	100pF
L_1	2.25pF
C_g	150pF
R_g	2.2kΩ

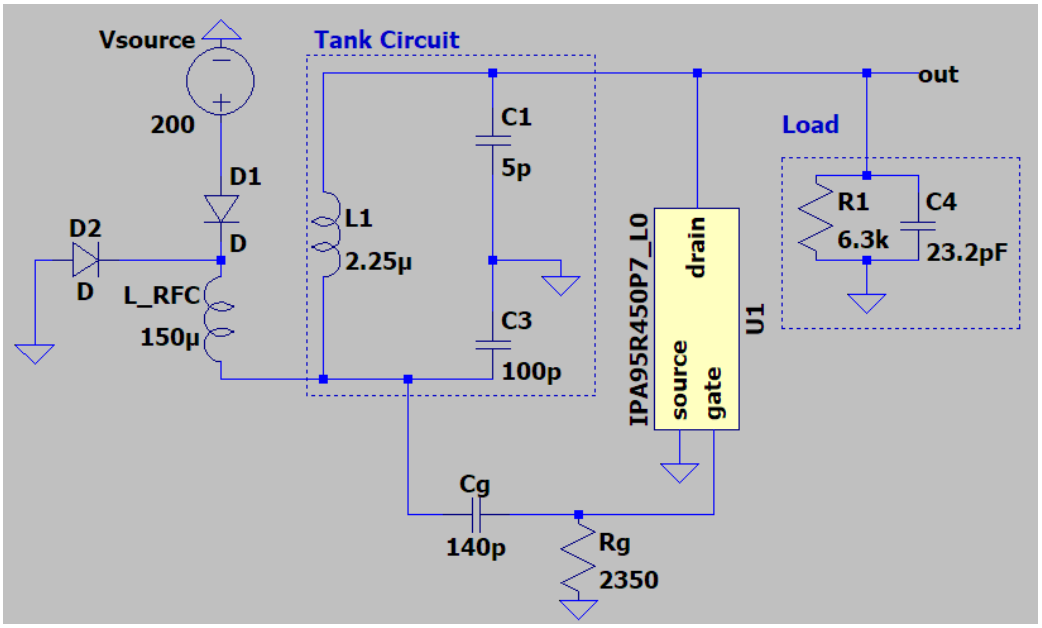

Fig. 14: Class C Amplifier Schematic

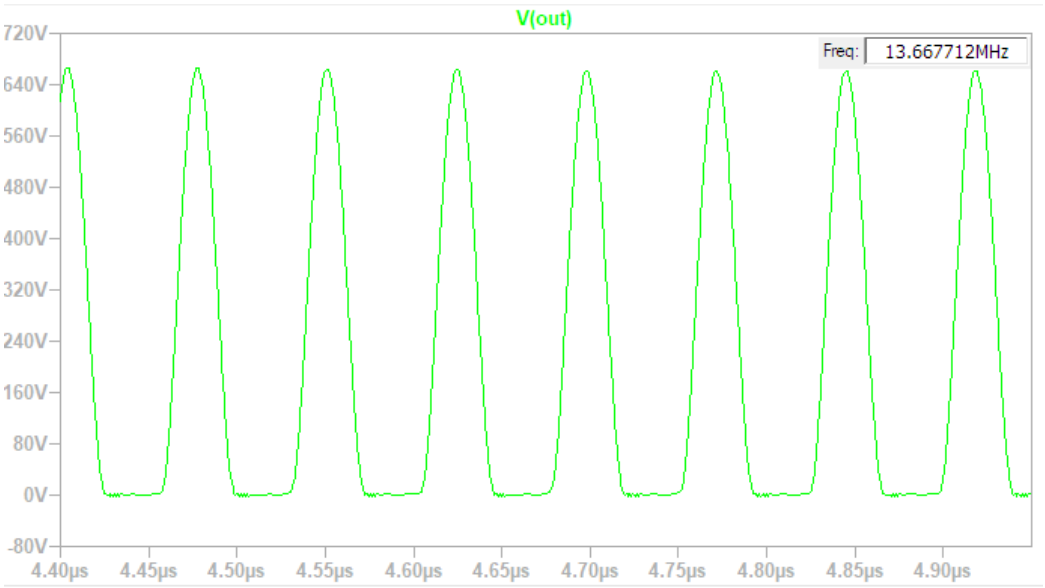

Fig. 15: Class C Amplifier Output With Adjusted Component Values (Output Frequency: 13.56MHz)

Using Table *2* and Fig. *14* values, the circuit operates at 13.67MHz with a peak of 682V (Fig. *15*). The self-excited amplifier's input current draw is 250A less than the non-self-excited design.

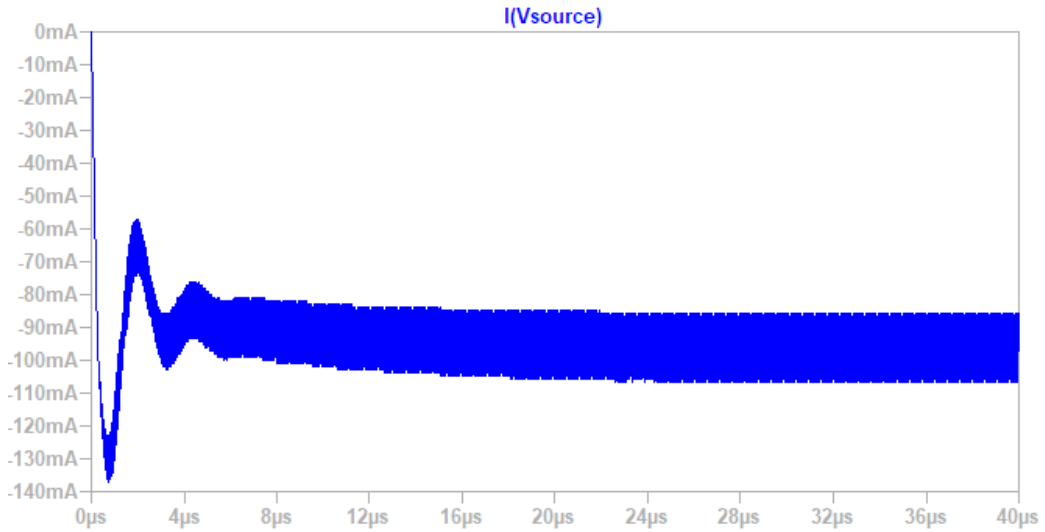

Fig. 16: Input Current to Self-Excited Class C Amplifier

Input current peaks at 130mA during startup then settles to 95.5mA during steady state while oscillating with an amplitude of 10.6mA and frequency of 13.67MHz (Fig. *16*). This input current is less than the maximum flyback converter output current (270mA).

Chapter 5: Food Chamber

To heat powdered food efficiently, a chamber for the food must facilitate even heating. Two designs are explored: a parallel plate capacitor or a cylindrical container.

5.1 Parallel Plate vs. Cylindrical Container

A cylindrical metal shell with centered electrode was designed in [2].

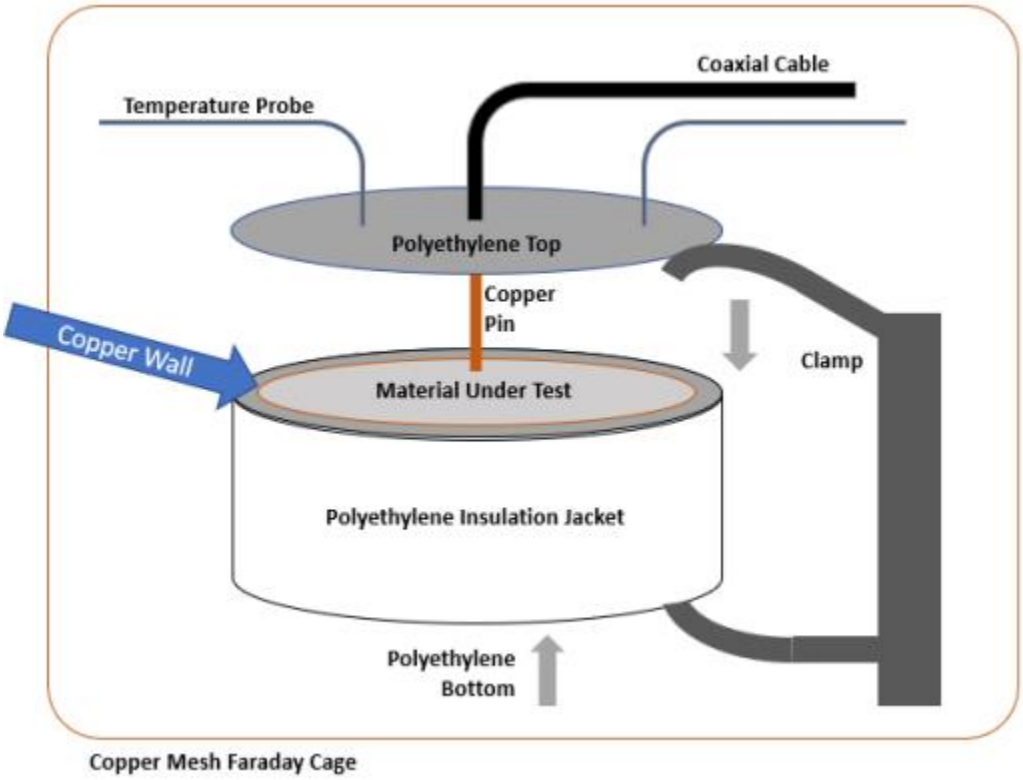

Fig. 17: Cylindrical Chamber Design [2]

This design creates an easy connection between the container and coaxial cable. The coax cable's center pin connects directly to the copper pin while the ground conductor is connected to the outer copper shell. The coax cable's

cylindrical chape is split and connected to the chamber. However, this design produces non-uniform electric fields.

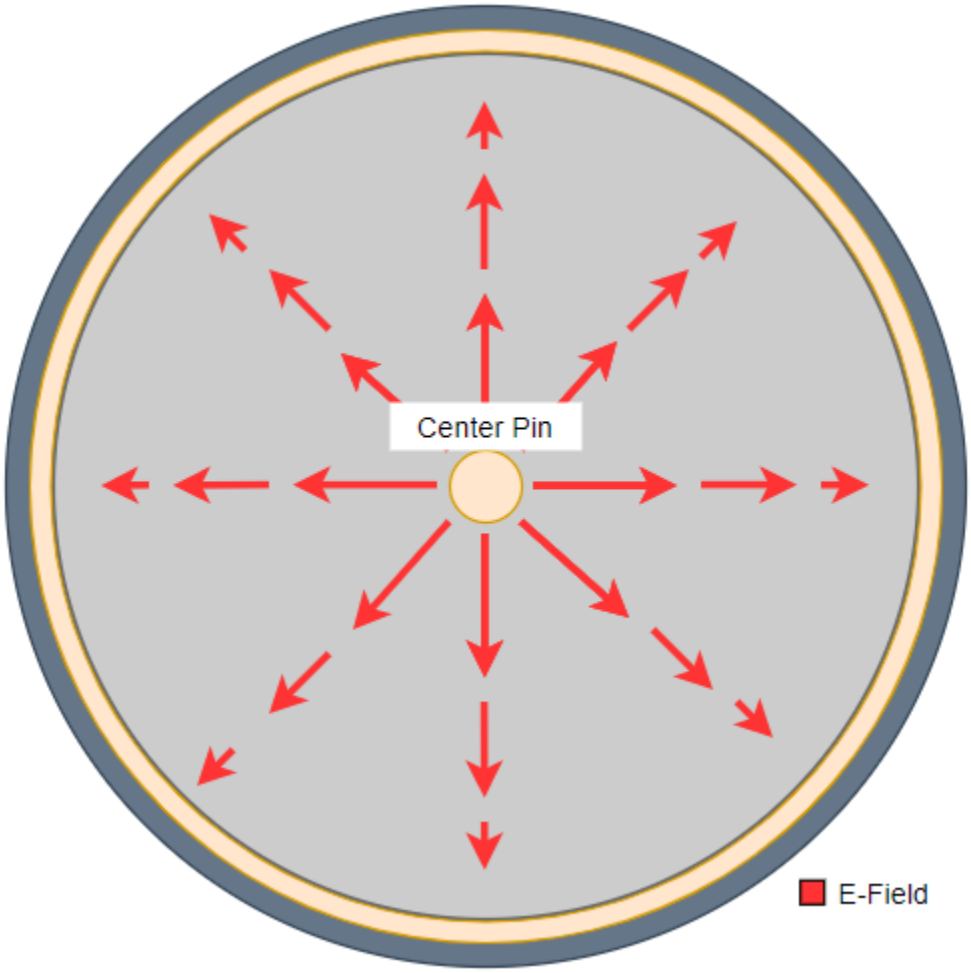

Fig. 18: Cylindrical Container Top-Down View

Fig. *18* shows the radiating electric fields from the center conductor to the surrounding copper shell. Electric field intensity decreases with distance from center conductor:

$$E = \frac{\lambda}{2\pi\varepsilon_0 R} \tag{16}$$

where λ is the signal's wavelength, ε_0 is the permittivity of free space, and R is center conductor to observation point distance. As the distance from the center pin increases, E-field power decreases at a rate of 1/R. This means the food at closest to the center conductor will heat up faster than the food further away. Uneven heating of food can lead to burning and discoloration before all of it can be pasteurized.

A common way to heat a volume of material evenly is to place it between two electrodes [12]. Parallel plates evenly distribute E-fields across the entire area of the plates (Fig. *19*).

Electromagnetic energy converted to thermal energy is described by:

$$P = 2\pi f \varepsilon_0 \varepsilon'' \, tan(\delta) \left|\vec{E}\right|^2 \tag{17}$$

where E is the electric field magnitude, ε_0 is the permittivity of free space, ε" is the dielectric loss factor, tan(δ) is the dielectric material's loss tangent, and f is the operating frequency.

5.1.1 Food Position Within the Chamber

The food position between the parallel plates plays an important role in how efficiently and effectively heating occurs. [12] shows that the electric fields deflect as follows.

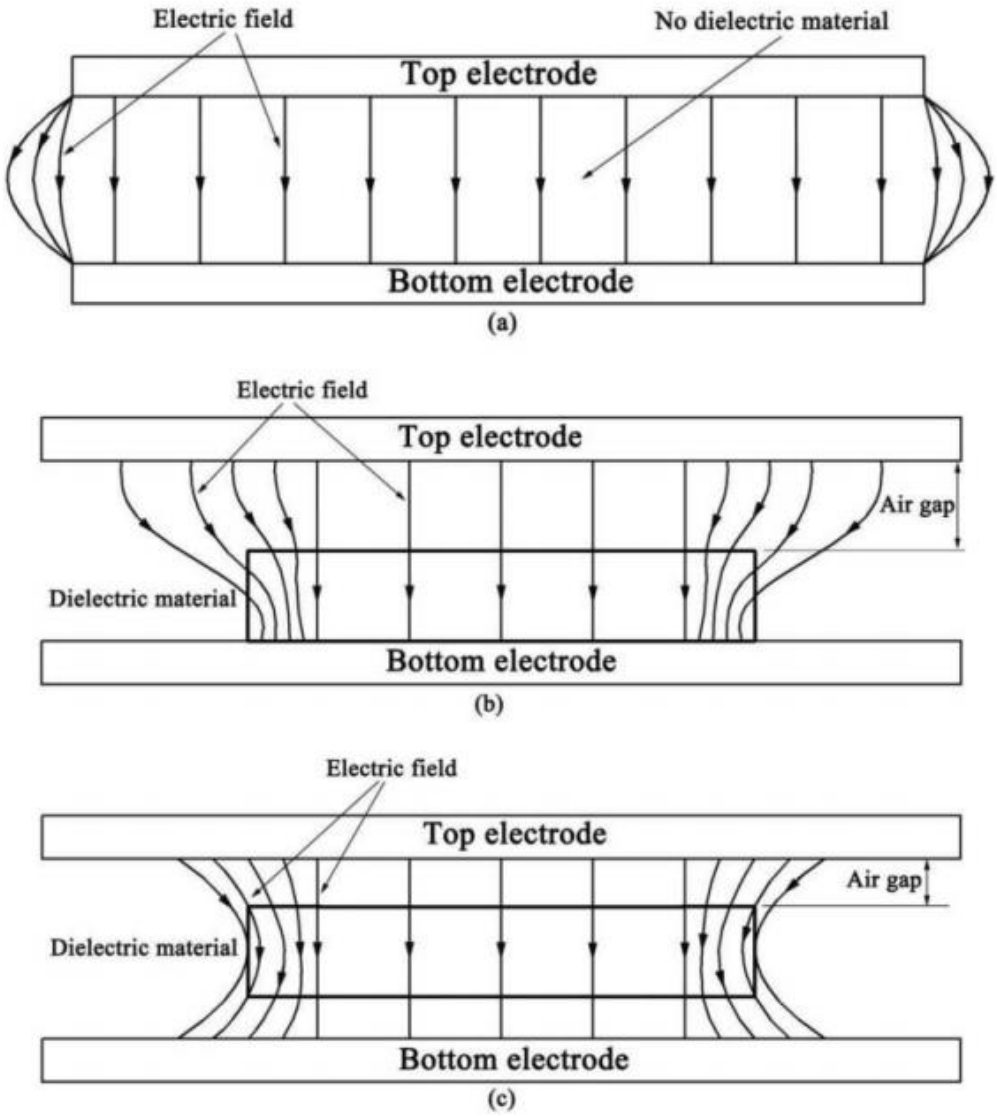

Fig. 19: Electric Field Strength Between Parallel Plates (a) no dielectric sample, (b) dielectric sample centered on bottom electrode, (c) dielectric sample placed in center between electrodes [12]

Non-uniform electric field distribution can result in non-uniform heating of food. Therefore, optimum size shape and food sample position maximizes electric field uniformity.

Fig. *19* (b) shows the food container in contact with the bottom electrode. The electric fields bend towards the food container, but the outermost E-field

lines enter the food through the middle instead of through the top. This creates a higher density of E-fields on the sides and bottom of the container. Fig. *19* (c) shows the food container placed equidistant from each electrode with an air gap between them. This causes the electric field to bend toward the food and creates a higher density of electric fields and more heating at the edges.

Maximizing the food container's cross-sectional area within plate boundaries also improved electric field uniformity [13]. A larger food container means the electric fields enter the food normally at the top face. Smaller containers cause oblique incidence electric at the container edges.

The air gap also plays a key role in food sample heating. A smaller gap between the plates and food sample results in faster food heating but less uniform heat distribution [14].

5.2 Equivalent Circuit Model

An equivalent circuit model simulates accurate load conditions for both the flyback converter and class C amplifier. Equations for both equivalent resistance and capacitance are derived in [15]. The equivalent capacitance of parallel plates is:

$$C = \frac{\varepsilon_0 \varepsilon_r' A}{d} \tag{18}$$

where ε_0 is the permittivity of free space, ε_r' is the dielectric constant, A is the area of each plate and d is the distance between the plates.

The equivalent load resistance is:

$$R = \frac{1}{2\pi f C_0 \varepsilon''} \tag{19}$$

where C_0 is the capacitance of free space and ε" is the dielectric loss factor. For parallel plate capacitors, C_0 is:

$$C_0 = \frac{\varepsilon_0 A}{d} \tag{20}$$

Table 3: Food Chamber Parameters

Parameter	Variable	Value
Plate Area	A	$0.105m^2$
Distance Between Plates	d	0.01m
Dielectric Constant of Wheat Flour	ε_r'	2.5
Loss Factor of Wheat Flour	ε"	0.187
Permittivity of Free Space	ε_0	$8.85x10^{-12}C/Nm^3$
Frequency	f	13.56MHz

Using Table *3*, the equivalent parallel capacitance and resistance was calculated for the parallel plate capacitor. The equivalent resistance and capacitance is 6.3kΩ and 23.2pF respectively.

The equivalent load circuit consists of a parallel resistor and capacitor. This model can be used in simulation to test the flyback converter and class C amplifier.

The dielectric constant (ε_r') and the loss factor (ε") change as a function of temperature [16]. From (20) and (21), as the food temperature increases, the equivalent resistance and capacitance will change proportionally.

5.3 Food Chamber

The food chamber includes two components: parallel plate electrodes and surrounding aluminum shielding.

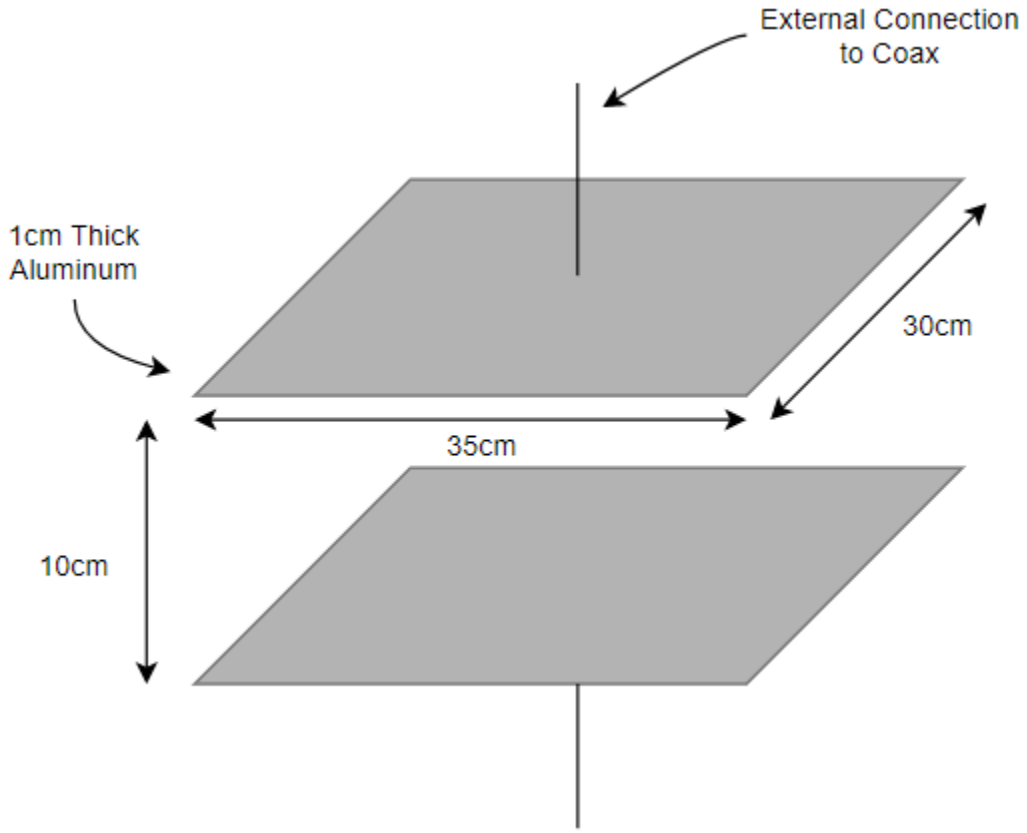

Fig. 20: Parallel Plate Design Dimensions

The aluminum plates connect to the class C amplifier though alligator clips. Each plate is 1cm in thick with a length of 35cm and a width of 30cm. To ensure safe operation, proper shielding is required around the capacitor to protect against the high-power RF radiation.

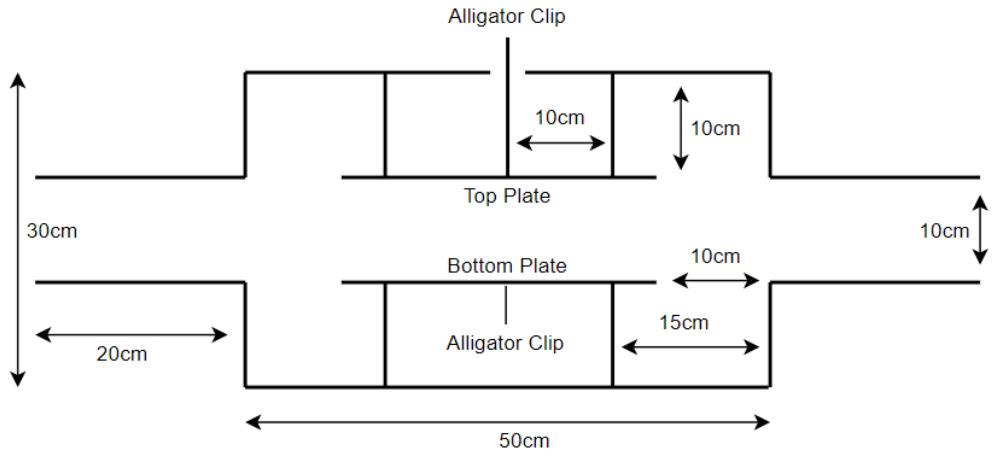

Fig. 21: Side View of Food Chamber and Aluminum Shielding

Chamber shielding is aluminum (Fig. *21*). Alligator clips enter the shielding through an open hole at the top. The left and right sides include small tunnels that pass through the entire chamber length. This allows for a conveyer system in future testing.

5.4 Parallel Plate Breakdown Voltage

Dielectric strength is the minimum voltage required to produce dielectric breakdown through a material [17]. Dielectric breakdown occurs when a sufficiently large voltage is present across a dielectric allowing charge to flow. The dielectric strength of the food material under test should be known to ensure no arcing occurs within the food chamber.

Breakdown voltage in air is [18]:

$$V_b = \frac{B * p * d}{ln(p * d) + k} \tag{21}$$

where p is the pressure, d is gap spacing between electrodes, B is related to the excitation and ionization energies, and k is [18]:

$$k = ln\left(\frac{A}{ln\,(1+\frac{1}{\gamma})}\right) \tag{22}$$

where A is the saturation ionization of the gas medium and γ is the secondary ionization coefficient. In air, A and B are 112.5 and 2737.5 respectively [18]. k can be found as a function of pd from Table *4*:

Table 4: Computed k as a Function of pd [18]

GAS	pd kPa-cm	k
AIR	0·0133-0·2	$2{\cdot}0583(pd)^{-0{\cdot}1724}$
	0·2 –100	$3{\cdot}5134(pd)^{0{\cdot}0599}$
	100–1400	4·6295 [CORRESPONDING TO pd=100 kPa-cm IN $k=3{\cdot}5134(pd)^{0{\cdot}0599}$]

where pd is the multiplication of the pressure p and gap distance d.

Air pressure at sea level is 101.325kPa and the gap spacing in the food chamber is 10cm leading to a pd of 1013.25kPa-cm. From Table 4, k is 5.3182.

Using (22), the breakdown voltage for a 10cm gap is 226.631kV and dielectric strength is 22.6kV/cm. Breakdown voltage of air is 50.43dBV greater than the output voltage of the class C amplifier. Therefore, arcing should not occur over the 10cm gap in the food chamber.

Ethylene tetrafluoroethylene, which has comparable characteristics to wheat flour, possesses a dielectric constant of 2.6 and dielectric strength of 2150kV/cm [19]. For a 10cm plate gap, the breakdown voltage would be

21.5MV and is 39.54dBV greater than the dielectric strength of air, providing sufficient margin for arc protection.

Chapter 6: Experimental Results

PCBs for the flyback converter and class C amplifier were designed and manufactured. Schematics and layout for both PCBs are shown in Appendix B and C. The food chamber was constructed by Jonathan Souza but due to time constraints and limited lab availability, testing was not able to be completed.

6.1 Flyback Converter

The flyback converter was constructed by Tim Erwin and is powered with a 24V power supply; 20A maximum continuous current (MEISHILE SM-247).

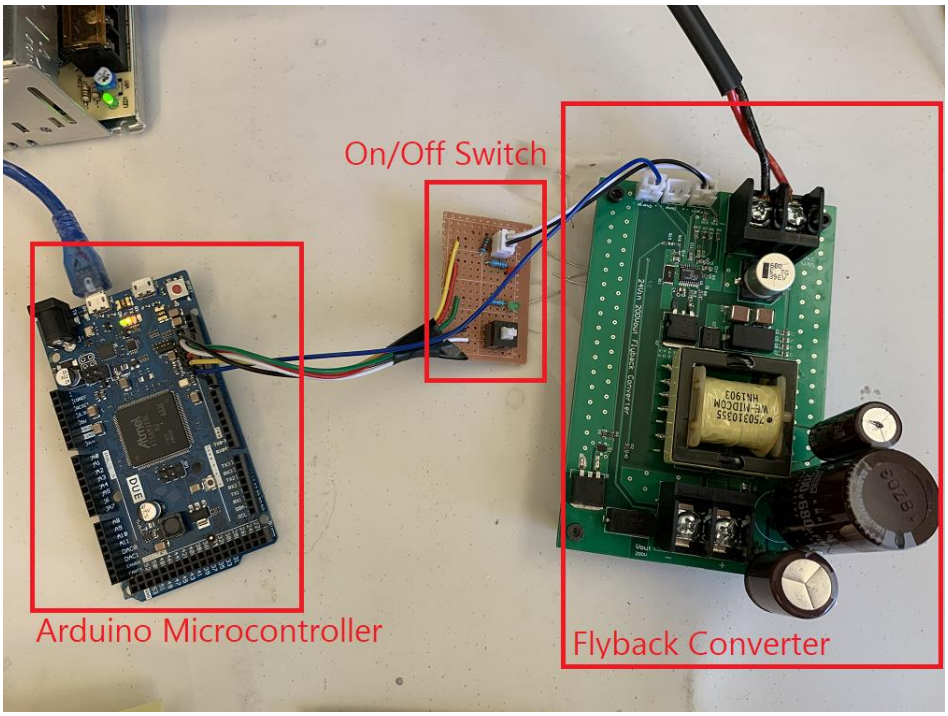

Fig. 22: Constructed Flyback Converter

An Arduino microcontroller powers LEDs on the on/off switch and monitors the charge status of the flyback controller. The green LED indicates the

flyback controller is ON and high voltage is present at the output. The red LED indicates the flyback is not switching properly and must be reset.

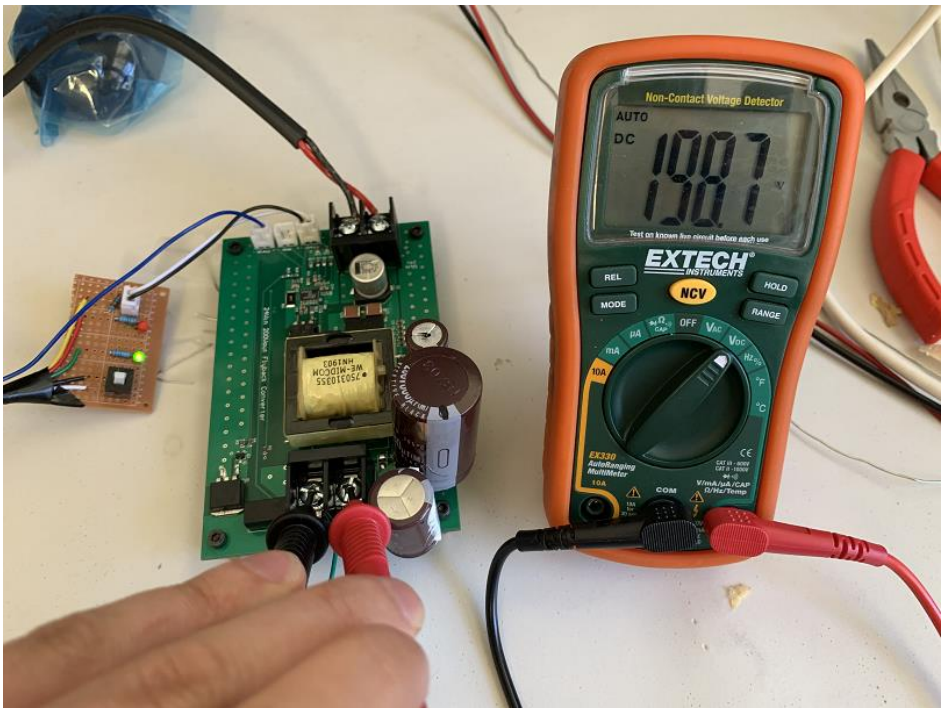

Fig. 23: Flyback Converter Output Voltage

While running, the flyback converter outputs 198.7V DC with no load. When a load is attached, the output voltage drops over time. This is due to the low capacitance on the output [19]. Adding more capacitors in parallel at the output could alleviate this problem, but more testing is needed to confirm.

6.2 Class C Amplifier

The class C amplifier was not tested with full load conditions due to time constraints. 0.25W resistors were used as a replacement load. Input voltage was lowered to 10V to decrease the power at the output. To operate properly at a lower voltage, the MOSFET was replaced with a 2N2222 transistor (Fig. *24*).

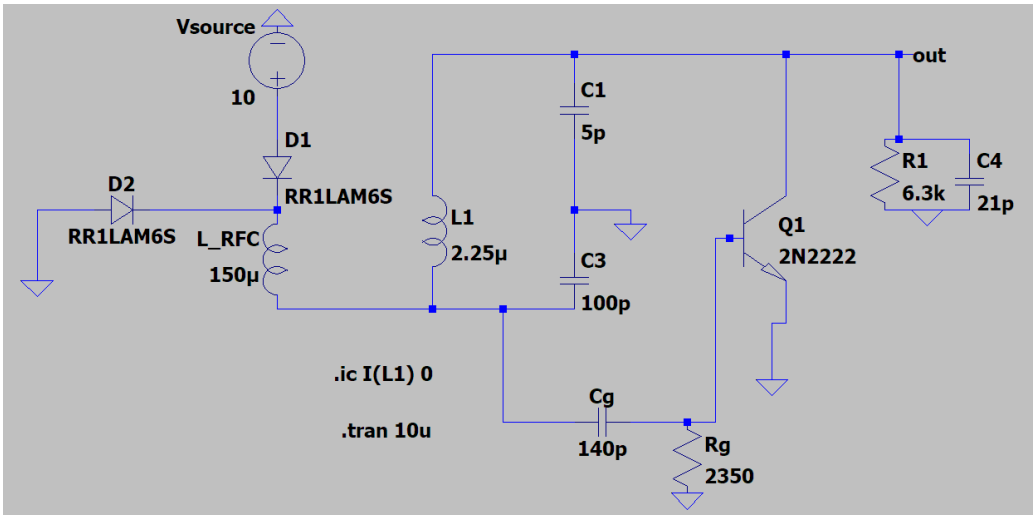

Fig. 24: Modified Class C Amplifier

Fig. 25: Modified Class C Amplifier Simulated Output Voltage

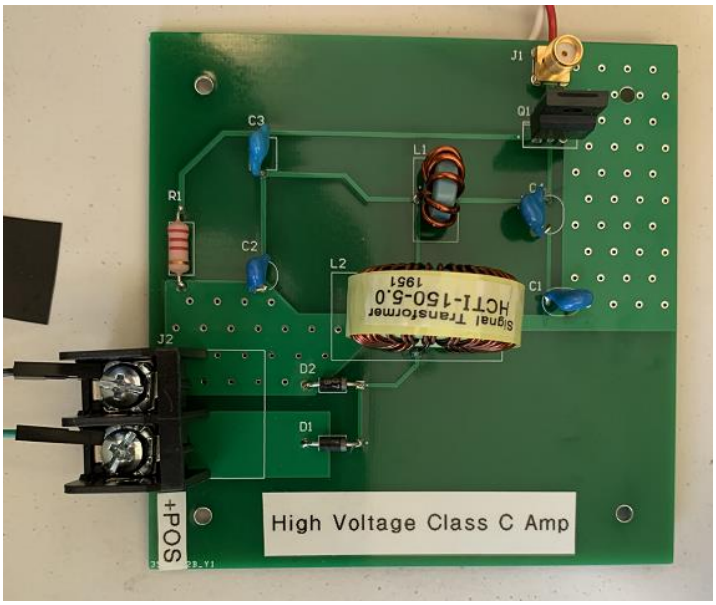

Fig. 26: Class C Amplifier PCB

LTSPICE simulations produced a modulated output voltage of 32V with a 10V DC input (Fig. *25*). During PCB testing, the output remained at 10V DC and did not modulate. Adding a capacitor in series with inductor L1 (Fig. *24*) may fix the output voltage problem, but further testing should be done for verification.

6.3 Food Chamber

The food chamber was constructed by Johnathan Souza. Limited access to tools and supplies made it difficult to build a robust chamber.

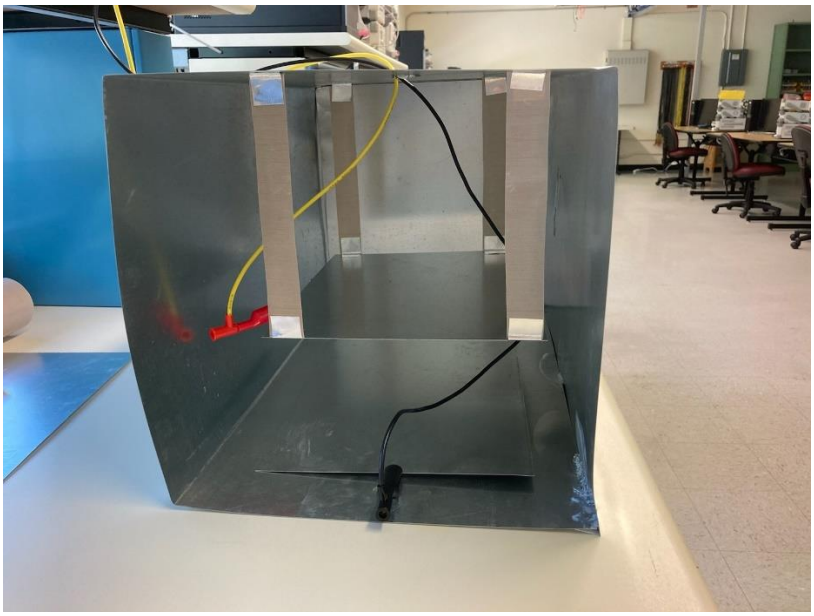

Fig. 27: Food Chamber (Internal View)

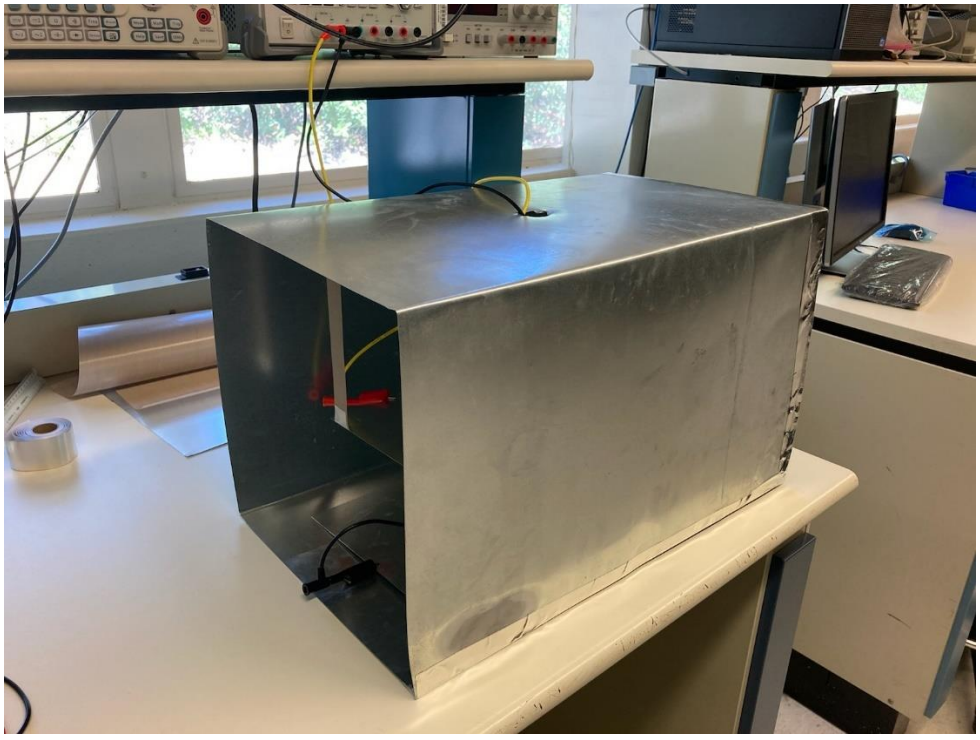

Fig. 28: Food Chamber (Side View)

Alligator clips enter through a hole at the top of the chamber and connect to both parallel plates. Limited lab availability restricted testing and proper chamber operation was not verified.

Chapter 7: Conclusions And Future Work

The system in this paper was created to develop a lower-power, commercially available device for low-moisture food pasteurization. Simulations verified the flyback converter and class C amplifier before PCB layout development.

7.1 Tradeoff Analysis Summary

Multiple trades are made in this paper to determine the best system configuration. All tradeoffs and rational are recorded in Table 5 below.

Table 5: System Tradeoffs

Subsystem	Configuration	Used in Final Design?	Rational
Operating Frequency	13.56MHz	Yes	Long wavelength provides more penetration depth. Lower frequency is easier to design and find parts.[1]
	27.12MHz	No	Shorter wavelength provides less penetration depth. Harder to find components. [1]
	40.68MHz	No	Shorter wavelength provides less penetration depth. Harder to find components.[1]
DC-DC Converter	Flyback Converter	Yes	High and low voltage isolation. Utilizes turns ratio of transformer to output higher voltage.
	Boost Converter	No	No voltage isolation. For same output voltage as flyback, a larger input is needed.
Class C Amplifier	Self-Excited	Yes	One input voltage. No frequency matching.
	External Reference	No	Two voltage sources needed. Frequency of reference needs to match exactly to resonance of tank circuit.
Food Chamber	Parallel Plates	Yes	Even distribution of E-fields for more even heating.
	Cylindrical Container	No	Uneven distribution of E-fields leads to uneven heating.

7.2 Future Work

The next step is to construct the PCBs and food chamber for a full system test. A full test would include measuring the bacterial concentration before and after food pasteurization to characterize pathogen reduction. Surrogate organisms can be used in place of harmful bacteria to mitigate risk of illness. A matching network may also be developed at the class C amplifier output to increase

[1] Penetration depth for poor conductors (such as flour) not explicitly determined.

efficiency and reduce output frequency variations to load conditions such as temperature and food density.

REFERENCES

[1] A. Altemimi, S. Aziz, A. Al-Hilphy, N. Lakhssassi, D. Watson and S. Albrahim, "Critical review of radio-frequency (RF) heating applications in food processing," *Food Quality and Safety,* vol. 3, no. 2, pp. 81-91, 2019.

[2] J. Sandoval, "The Characterization of Effective Electromagnetic Fields on the Safety and Quality of Low-Moisture Foods (EFFS) – Prototype Device Development," California Polytechnic University, San Luis Obispo, 2020.

[3] A. Sanchez-Maldonado, A. Lee and J. Farber, "Methods for the Control of Foodborne Pathogens in Low-Moisture Foods," *Annual Revew of Food Science Technology,* vol. 9, pp. 177-208, 2018.

[4] C. Pan, "Detection of bacterial pathogens in low moisture foods with Dual Immunological Raman-Enabled Crosschecking Test (DIRECT) and Raman mapping," Iowa State University, Ames, 2020.

[5] *21 CFR 120.24 Revised as of April 1, 2020.*

[6] "PSC Heating & Drying with Radio Frequency," 17 June 2020. [Online]. Available: https://www.pscrfheat.com/products/rf-convection-combination-systems/.

[7] M. S. Ferdous, "DESIGN OF A RADIOFREQUENCYHEATING SYSTEM FOR ELECTROLYTIC LIQUIDS AND SLUDGES," University of British Columbia, Vancouver, 2015.

[8] E. Lindstorm, L. Garcia-Rodriguez, A. Oliva and J. Balda, "Designing an Optimum Non-Dissipative LC Snubber for Step-Up Flyback Converters in DCM," *2017 IEEE 8th Latin American Symposium on Circuits & Systems (LASCAS),* pp. 1-4, 2017.

[9] R. Ridley, "Flyback Converter Snubber Design," *Switching Power Magazine,* pp. 1-7, 2005.

[10] Analog Devices;, "High Voltage Capacitor Charger Controller with Regulation," 2017.

[11] M. Heydari, S. Mirhoseini, H. Mohammadpour and A. Shoulaie, "Analytical & experimental studies on impedance matching in RF generators for dielectric loads," *2009 International Conference on Power Engineering, Energy and Electrical Drives,* pp. 37-42, 2009.

[12] Z. Huang, F. Marra, J. Subbiah and S. Wang, "Computer simulation for improving radio frequency (RF) heating uniformity of food products: A

review," *Critical Reviews in Food Science and Nutrition,* vol. 58, no. 6, pp. 1033-1057, 2017.

[13] G. Tiwari, S. Wang, J. Tang and S. Birla, "Analysis of radio frequency (RF) power distribution in dry food materials," *Journal of Food Engineering,* vol. 104, no. 4, pp. 548-556, 2011.

[14] R. Uyar, F. Erdogdu, F. Sarghini and F. Marra, "Computer simulation of radio-frequency heating applied to block-shaped foods: Analysis on the role of geometrical parameters," *Food and Bioproducts Processing,* vol. 98, pp. 310-319, 2016.

[15] F. Marra, L. Zhang and J. Lyng, "Radio frequency treatment of foods: Review of recent advances," *Journal of Food Engineering,* vol. 91, no. 4, pp. 497-508, 2009.

[16] B. Lin and S. Wang, "Dielectric properties, heating rate, and heating uniformity of wheat flour with added bran associated with radio frequency treatments," *innovative Food Science & Emerging Technologies,* vol. 60, 2020.

[17] A. Shrivastava, Introduction to Plastics Engineering, Amsterdam: Elsevier Inc., 2018.

[18] E. Husain and R. Nema, "Analysis of Paschen Curves for air, N2 and SF6 Using the Townsend Breakdown Equation," *IEEE Transactions on Electrical Insulation,* Vols. EI-17, no. 4, pp. 350-353, 1982.

[19] T. Erwin, *private communication,* 2021.

[20] P. Meng, X. Wu, J. Yang, H. Chen and Z. Qian, "Analysis and design considerations for EMI and losses of RCD snubber in flyback converter," *Proc. of the Twenty-Fifth Annual IEEE Applied Power Electronics,* p. 642–647, 2010.

[21] R. Petkov and L. Hobson, "Analysis and optimisation of a flyback convertor with a nondissipative snubber," *Proc. of the IEEE Electric Power Applications,* vol. 142, no. 1, pp. 35-42, 1995.

[22] S.-G. P. Plastics, *Norton ETFE Fluoropolymer Film,* 2002.

APPENDICES

Appendix A: LT3751 Datasheet Schematic

BLOCK DIAGRAM

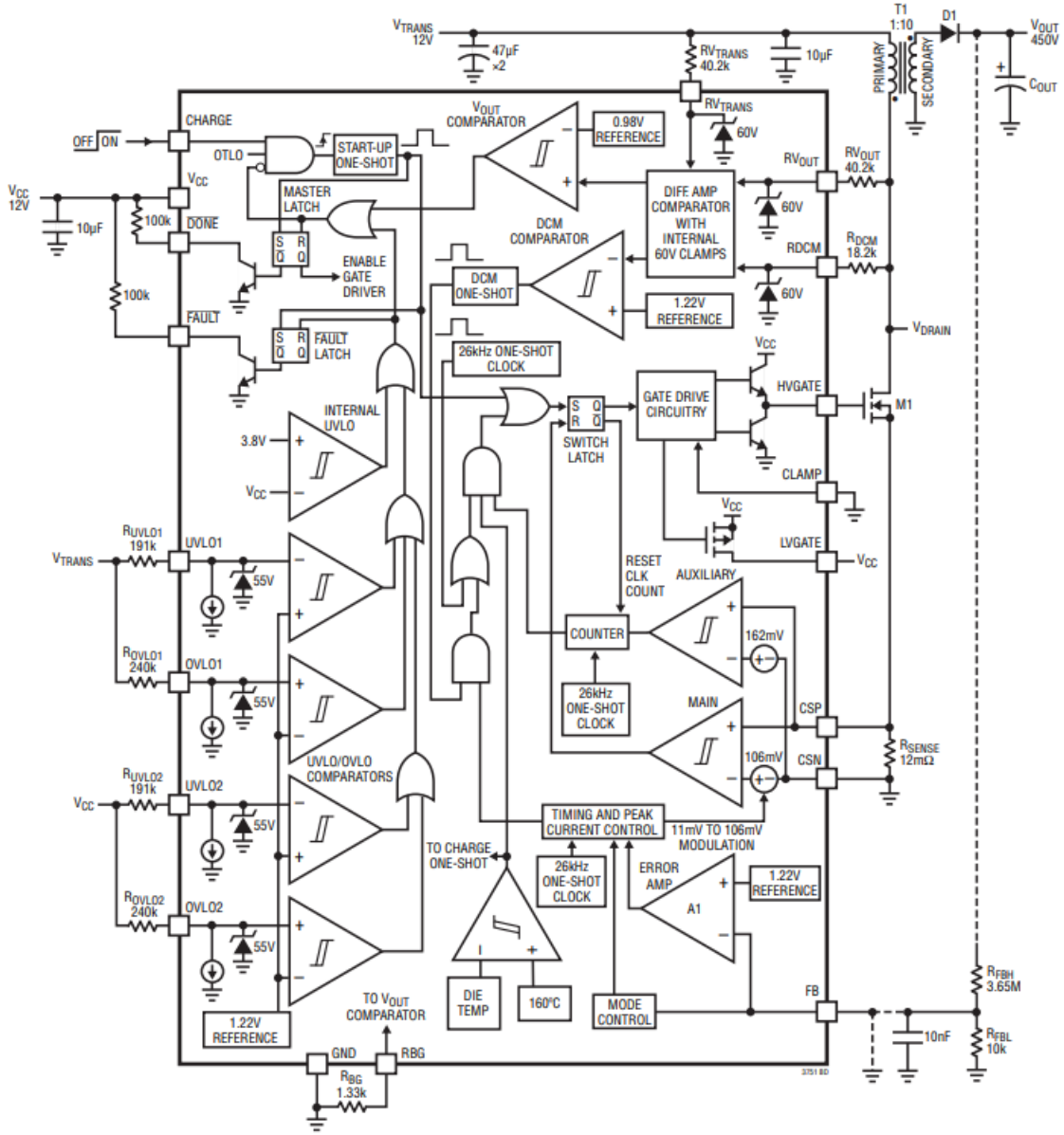

Fig. 29: LT3751 Block Diagram

Appendix B: Flyback Converter Schematics and PCB

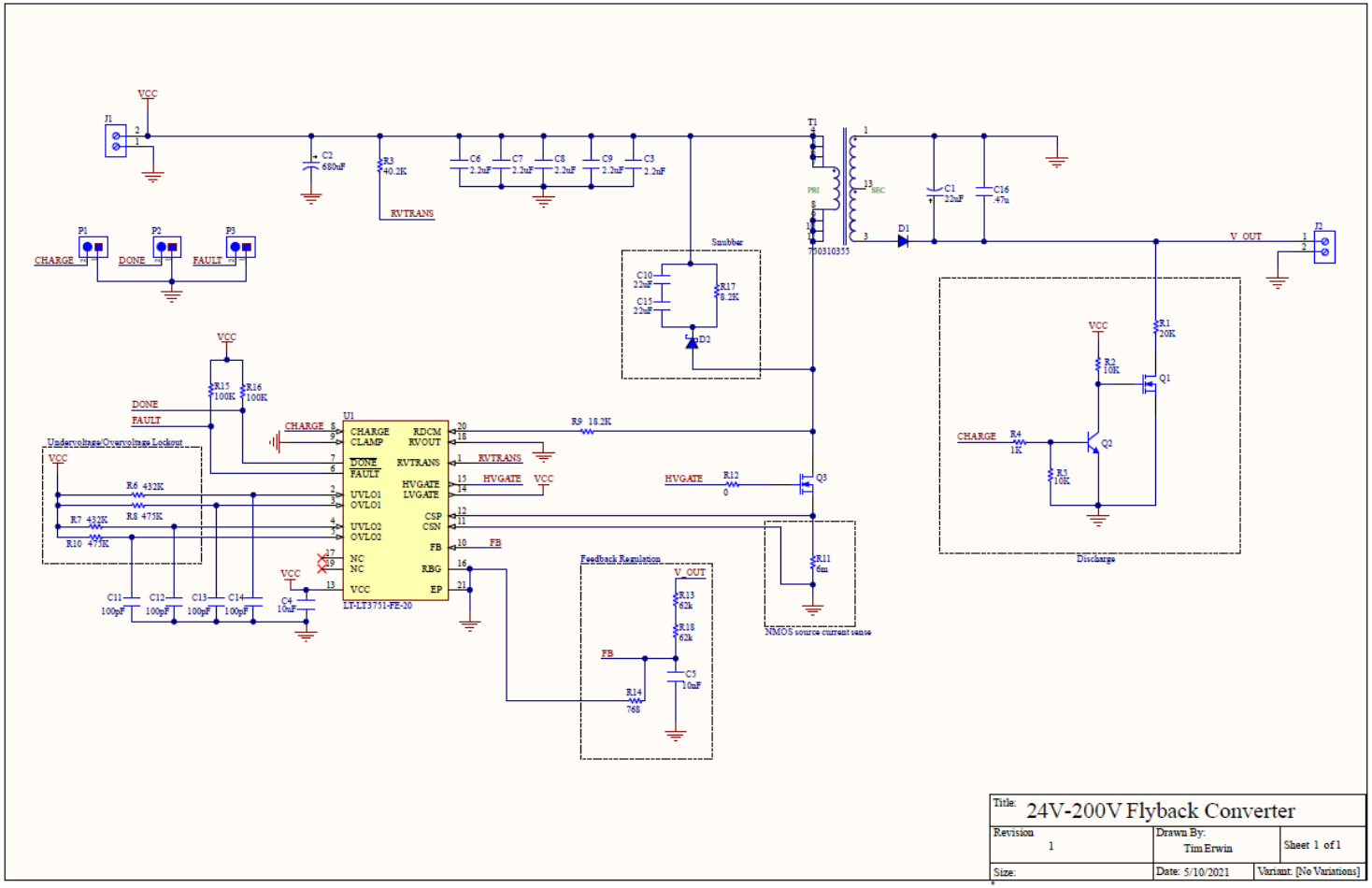

Fig. 30: Flyback Converter PCB Schematic

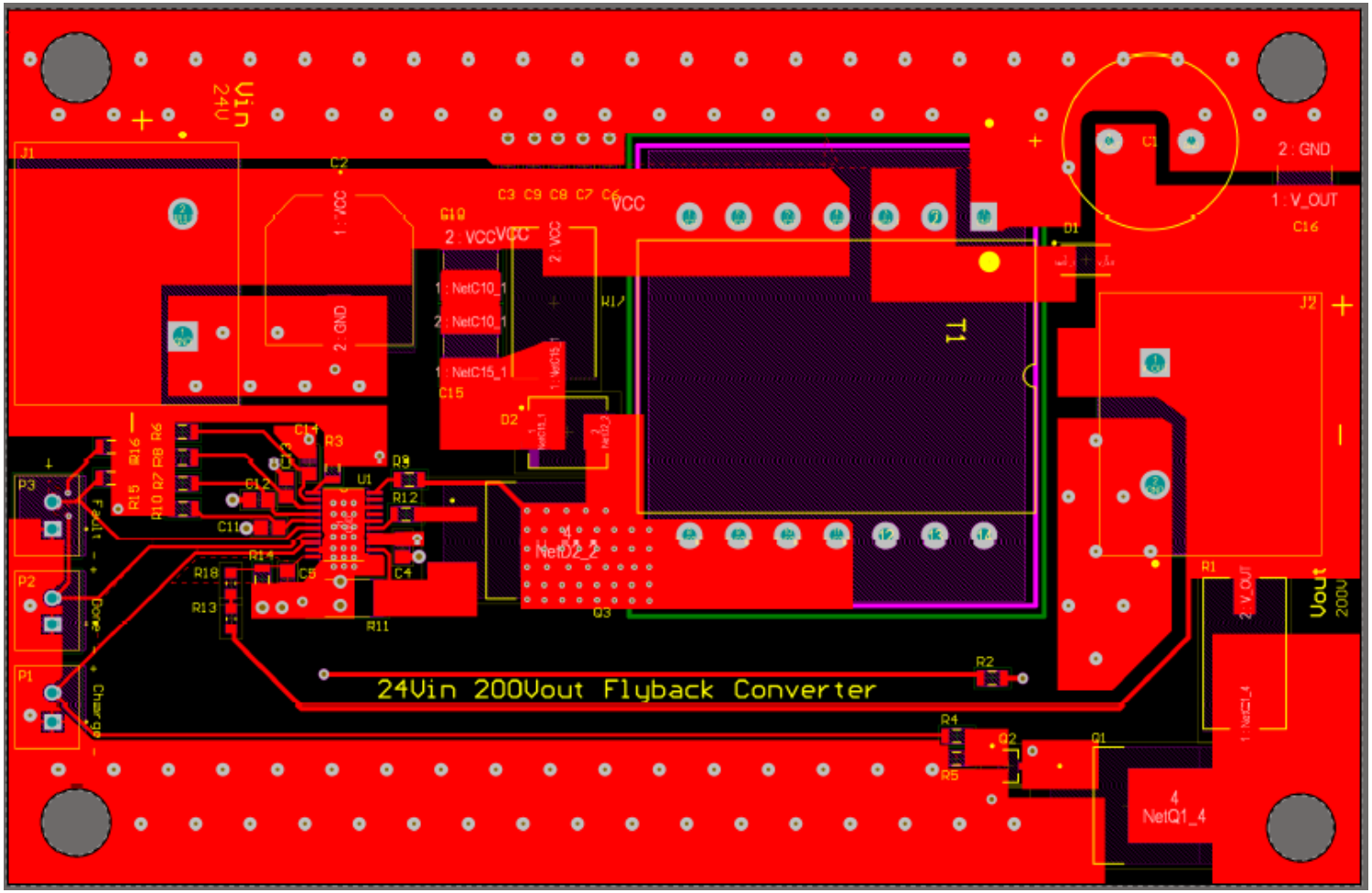

Fig. 31: Flyback Converter PCB Layout (Top)

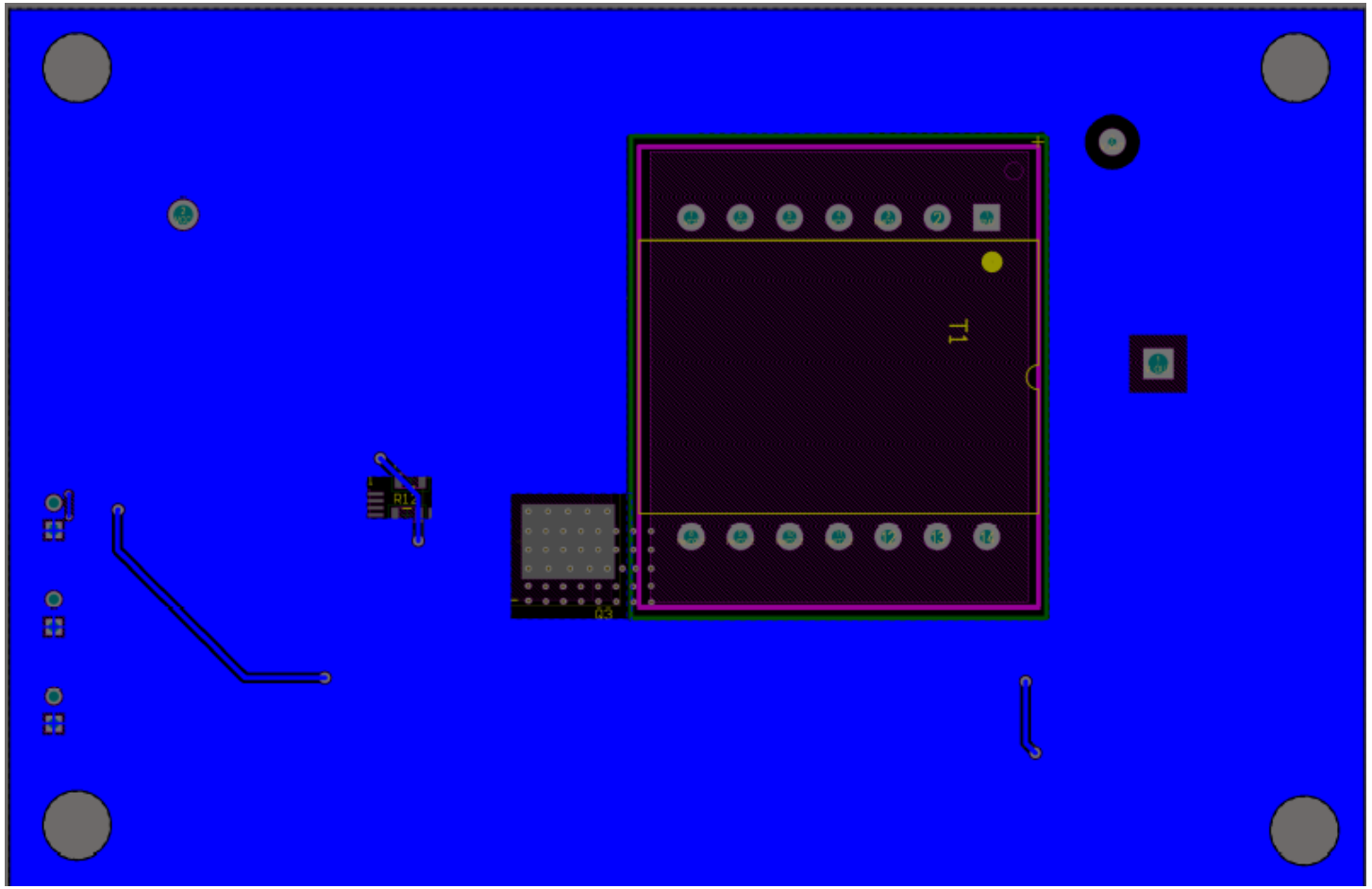

Fig. 32: Flyback Converter PCB (Bottom)

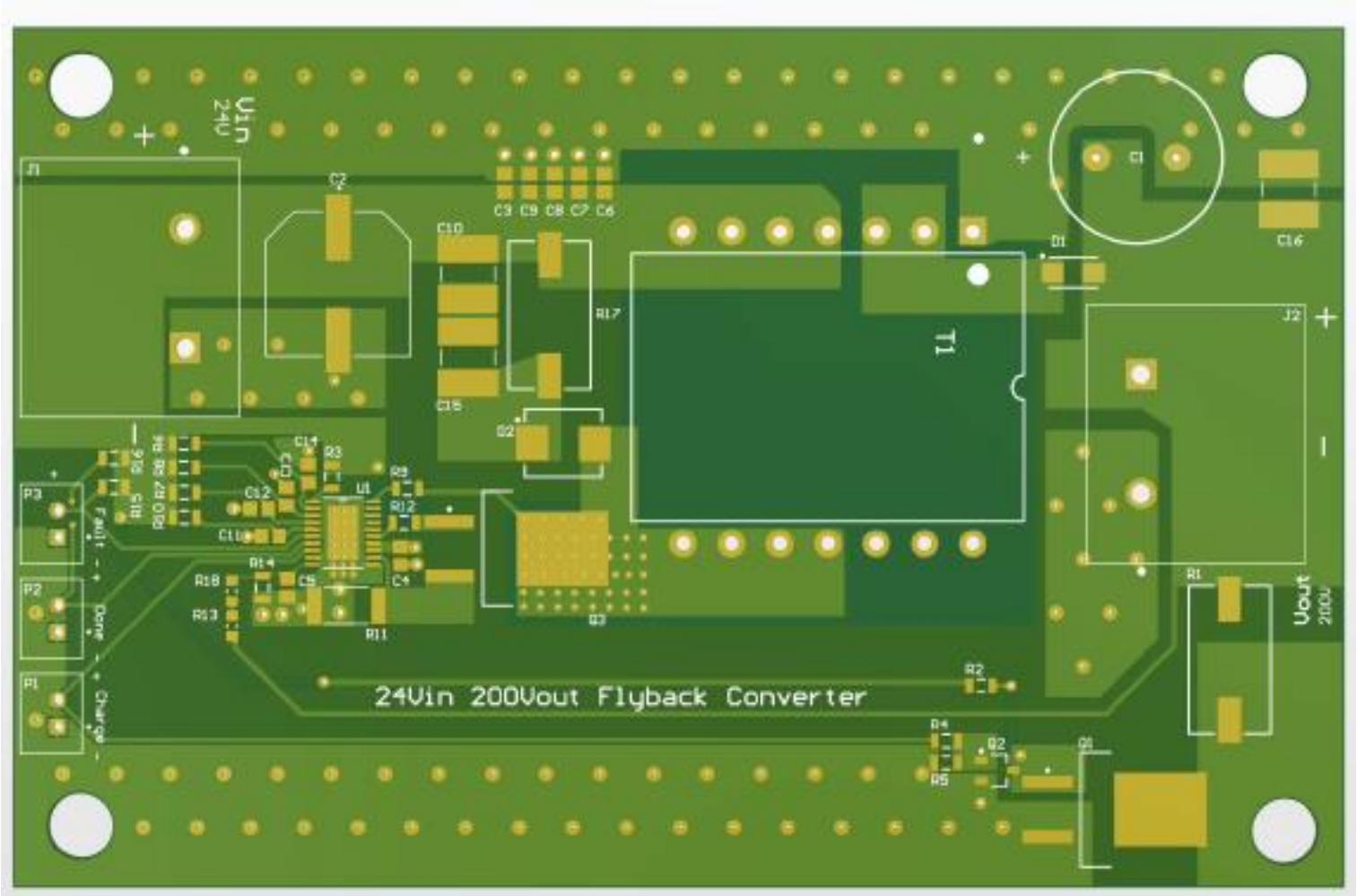

Fig. 33: Flyback Converter PCB Layout

Appendix C: Class C Amplifier Schematic and PCB

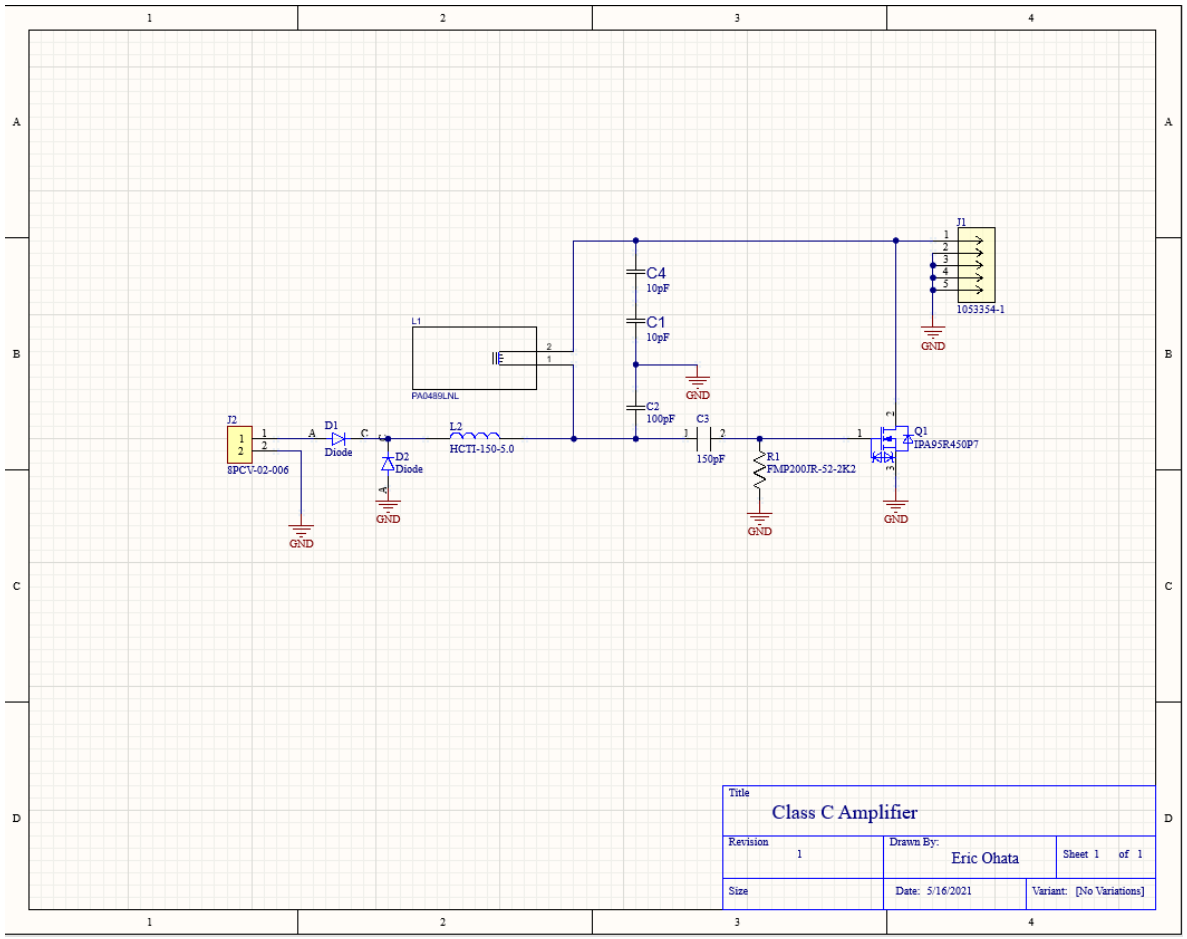

Fig. 34: Class C Amplifier PCB Schematic

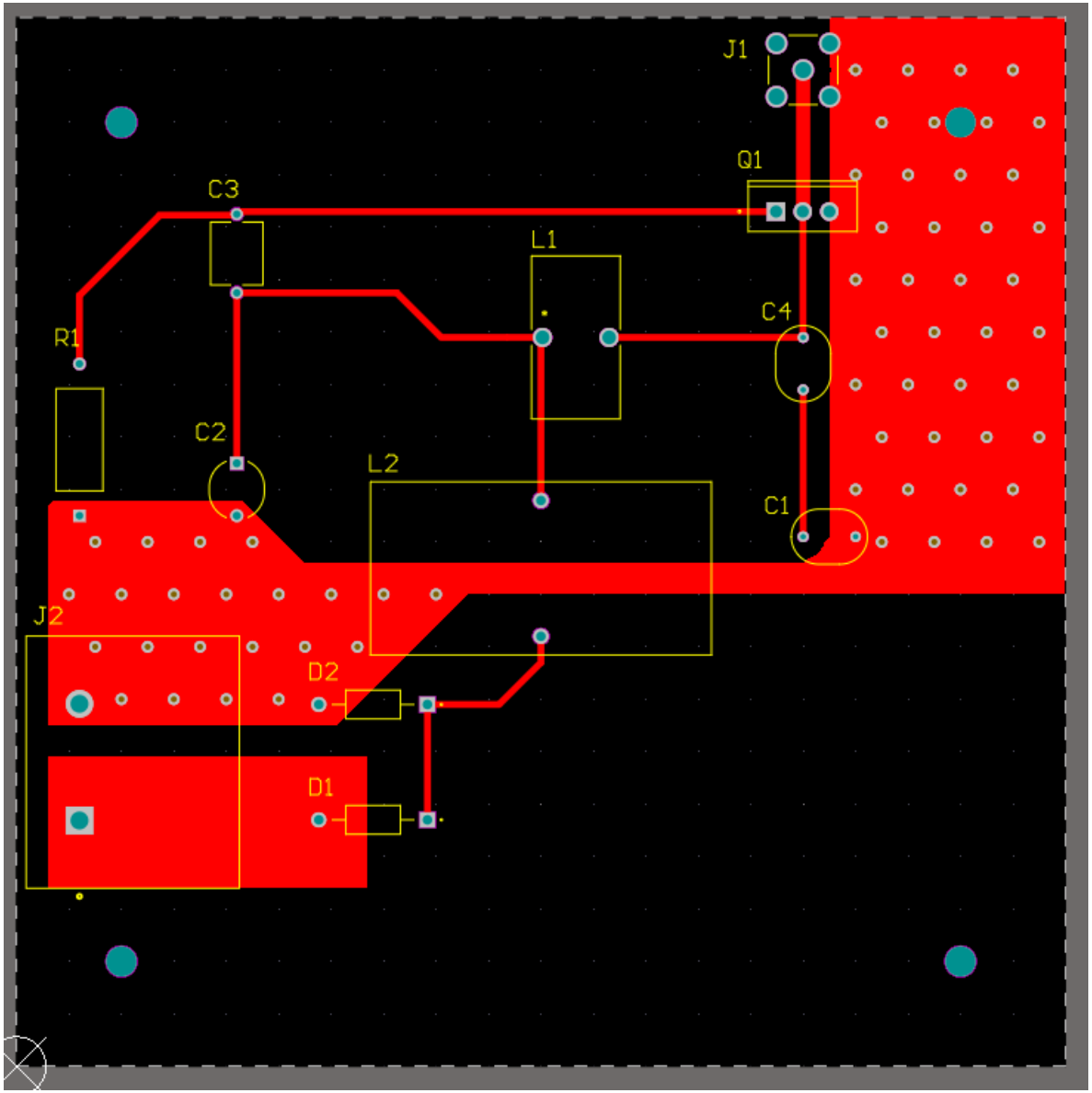

Fig. 35:Class C Amplifier PCB Layout (Top)

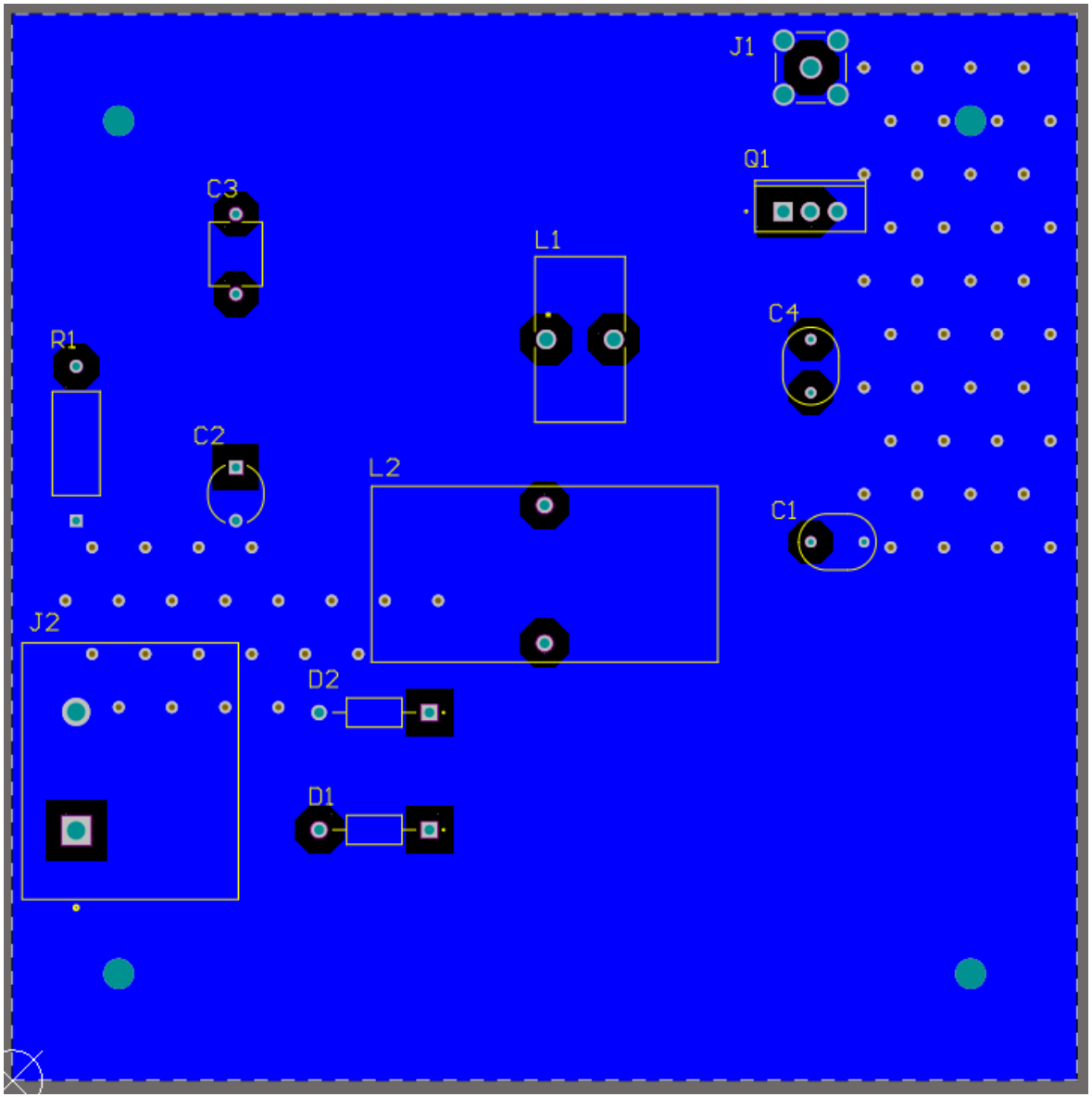

Fig. 36: Class C Amplifier PCB Layout (Bottom)

Appendix D: Flyback Converter BOM

Designator	Type	JLCPCB Part # and li	JLCPCB Price	Digikey Part # and li	Price	Description	Quanitity for 1	JLCPCB Total	Digikey Total2	Notes
	300V regulator									
U1	IC	C671372	$9.5200	LT3751	$8.64	High voltage regulator controlle	1	$9.5200	$8.64	
Q3	Transistor	--	--	FQB19N20L	$1.57	nMOSFET	1	--	$1.57	
T1	Transformer	--	--	732-2131-ND	$12.10	Flyback Power Transformer	1	--	$12.10	
C11-14	Capacitor	CL21C101JBANNNC	$0.0117	8.85012E+11	$0.10	100pF, ceramic	4	$0.0468	$0.40	
C5	Capacitor	CL21B103KBANNN	$0.0107	C0805X103K1RAC331	$0.14	10nF, 50V, ceramic, 0805	1	$0.0107	$0.14	
C3	Capacitor	0805F225M500NT	$0.0293	08053C225KAT4A	$0.33	2.2uF, 25V, ceramic	5	$0.1465	$1.65	
C1	Capacitor	--	--	UCA2G220MHD6TN	$1.59	22uF, 400V, electrolytic	1	--	$1.59	
C4	Capacitor	CL21A106KAYNNNE	$0.0259	GRM21BR61H106ME	$0.42	10uF, 25V, ceramic	1	$0.0259	$0.42	
C2	Capacitor	--	--	EEV-TG1E681UQ	$1.65	680uF, 25V, electrolytic	1	--	$1.65	
C16	Capacitor	--	--	CKG57NX7R2J474M5	$4.09	0.47uF, 630V, ceramic	1	--	$4.09	
R11	Resistor	--	--	PMR100HZPFU6L00	$0.70	6m, current sense	1	--	$0.70	
R14	Resistor	C17823	$0.0042	RMCF0805FT1K13	$0.10	768, 0805	1	$0.0042	$0.10	
R9	Resistor	0805W8F1822T5E	$0.0038	RMCF0805FT18K2TR	$0.10	18.2K, 0805	1	$0.0038	$0.10	
R3	Resistor	0805W8F4022T5E	$0.0043	2019-RK73H2ATTD4(	$0.10	40.2K, 0805	1	$0.0043	$0.10	
R11	Resistor			ERJ-PB3D6202V	$0.16	62k, 0603, 1/5W	2	$0.0000	$0.32	
R6-7	Resistor	0805W8F4323T5E	$0.0040	RMCF0805FT432KTR	$0.10	432K, 1% 0805	2	$0.0080	$0.20	
R8,10	Resistor	0805W8F4753T5E	$0.0040	RK73H2ATTD4753F	$0.10	475K, 1%, 0805	2	$0.0080	$0.20	
R15,16	Resistor	0805W8F1003T5E	$0.0040	RMCF0805FG100K	$0.10	100k, 0805 Pullup for Done and F	2	$0.0080	$0.20	
D1	Diode	C412437	$0.0138	US1MHE3_A/H	$0.42	1000V output diode	1	$0.0138	$0.42	
	Resistor	--	--	CRCW08050000Z0EA	$0.21	0, 0805 gate resistor	1	--	$0.21	
	Flyback Snubber									
D2	Diode	--	--	ucts/detail/on-sem	0.66	Schottky	1	--	$0.66	
C10,15	Capacitor	--	--	A226M500JJ/3934246	$5.44	22uF	2	--	$10.88	
R17	Resistor	--	--	detail/te-connectiv	$0.56	8.2k, 5W	1	--	$0.56	
	Charge Enable									
P1,2,3	Pin Header Male	--	--	455-2247-ND	$0.15	Connector Header Through Hole	3		$0.45	
	Discharge									
Q1	Transistor	--	--	FQB5N60CTM-WS	$1.29	NMOSFET, 600V	1	--	$1.29	
Q2	Transistor	--	--	2SCR553R	$0.50	NPN	1	--	$0.50	
R4	Resistor	C17513	$0.0040	CR0805-JW-102ELF	$0.10	1K, 0805 for NPN base	1	$0.0040	$0.10	
R2,5	Resistor	C17414	$0.0040	RMCS0805JT10K0	$0.10	10K, Pulldown and Vcc	2	$0.0080	$0.20	
R1	Resistor	--	--	SMF520KJT	$0.93	20K, SMT, discharge resistor	1	--	$0.93	
	In/Out									
J1,2	Connector	--	--	8PCV-02-006	$1.84	High voltage screw terminal	2	--	$3.68	
	Wire	--	--	https://www.showi	$1.42	14 AWG, 600V, 25A, 1ft	5	--	$7.10	

Appendix E: Class C Amplifier BOM

Comment	Description	Designator	Footprint	LibRef	Quantity	Digi-Key Part Number	Unit Price	Total Price
CC45SL3JD100JYVNA	10pF	C1, C4	CC45SL3JD100JYVNA	CC45SL3JD100JYVNA	2	445-181005-1-ND	$0.50	$1.00
CK45-R3AD101K-NRA	100pF	C2	CK45-R3AD101K-NRA	CK45-R3AD101K-NRA	1	445-16009-ND	$0.42	$0.42
DE2B3SA151KN3AY02F	150pF	C3	CAP_DE2B3SA151KN3AY02F	DE2B3SA151KN3AY02F	1	490-16222-1-ND	$0.61	$0.61
UF4007	75ns, 1A, 1000V, High Efficient Recovery Rectifier	D1, D2	DIOAD1036W78L520D274	UF4007	2	UF4007TR-ND	$0.43	$0.86
1053354-1	2062 0000 00,SMA PCB VERT JACK	J1	conn5_1053354-1_TEC	1053354-1	1	A30046-ND	$12.68	$12.68
8PCV-02-006	2 Circuit 0.438 _11.12mm_ Barrier Block Connector, Screws with Captive Plate	J2	TE_8PCV-02-006	8PCV-02-006	1	A98460-ND	$1.89	$1.89
PA0489LNL	2.24uH	L1	PA0489LNL_PUL	PA0489LNL	1	553-1507-ND	$1.33	$1.33
HCTI-150-5.0	High Current Toroidal Inductor	L2	IND_HCTI-150-5.0	HCTI-150-5.0	1	595-1730-ND	$2.44	$2.44
IPA95R450P7	Insulated-Gate Field-Effect Transistor (IGFET), N-Channel, Enhancement, Body Diode, ESD Diode Gate/Source, Pin 1 Gate, 2 Drain, 3 Source, 3 Pins	Q1	IPA95R450P7	IPA95R450P7	1	Available on Infineon Website	$2.91	$2.91
FMP200JR-52-2K2	2.2kohm	R1	YAG_FMP200_YAG	FMP200JR-52-2K2	1	2.2KZCT-ND	$0.31	$0.31
Total Cost:	$30.66							

Appendix F: Food Chamber BOM

Chamber parts list:

Item/Quantity	Store	Cost
3 Pack PTFE Teflon sheets	Amazon.com	$8.89
1ft x 2ft 3/8” aluminum plate	Metals Depot	$105.36
36in x 36in aluminum sheet (x3)	Home Depot	$71.04
RG174 2ft coaxial cable (BNC)	L-com	$10.07
WK2301 Propane Torch Kit*	Home Depot	$20.97
AL3 aluminum brazing rods	Home Depot	$4.97
6-1/2” tooth aluminum metal cutting blade*	Home Depot	$34.97
Total Cost:		**$256.27**